Evaluation of the epidemiological outlook of the influenza A/H3N2 clade K in England during the 2025-26 season

James A Hay[*,1], Punya Alahakoon[†,1], Alexander Greenshields-Watson[†,1], Michelle Kendall[1], Mahan Ghafari[1,2], Chris Wymant[1], Robert Hinch[1], Luca Ferretti[1], Jasmina Panovska-Griffiths[1,3,4], Christophe Fraser[1]

1. Pandemic Sciences Institute, Nuffield Department of Medicine, University of Oxford, Oxford, UK
2. Department of Biology, University of Oxford, Oxford, UK
3. The Queen's College, University of Oxford, Oxford, UK
4. UK Health Security Agency, London, UK

* Correspondence to james.hay@ndm.ox.ac.uk
† Contributed equally

Key findings

- England is currently experiencing a high growth rate of infections caused by the influenza A/H3N2 K clade. Antigenic change from the previously dominant clade, a rapid selective sweep evident in genomic data, and an unusually early start to the season have raised concerns about the potential severity of this year's influenza season.
- Analysis of publicly available data sources from the current season suggests that the effective reproduction number has been largely consistent with previous severe seasons. However, the modelled peak growth rate in the current season to date is slightly higher than previous peak growth rates from the past 10 years when subsetting for A/H3N2 cases, but comparable when aggregating all influenza cases.
- Scenario analyses using an age-stratified compartmental model compared to the previous A/H3N2 season in 2022/23 suggest that substantial immune escape is unlikely given current epidemiological trends. Current trends are compatible with small levels of immune escape in all ages, or slightly greater immune escape in children, or a 10-20% higher R_0, or an earlier seed date with no change in virus fitness or immune escape. In almost all scenarios, an earlier and faster epidemic growth rate leads to depletion of susceptibles before the Christmas period with a dampening effect due to the half term school holiday.
- To support understanding and exploration of model outputs, an interactive visualisation tool was devised and made available online: https://hay-idd.shinyapps.io/ModelFluUk-H3N2/
- This rapid analysis is intended to support situational awareness. It provides quantitative comparisons of early epidemic growth rates with previous seasons and qualitative insights into plausible epidemic dynamics.

Introduction

The 2025/26 influenza season in the northern hemisphere appears to be dominated by an antigenically drifted clade of A/H3N2 viruses. This clade—named K (previously J.2.4.1)—is descended from the J.2 clade on which the vaccine strain selection was based, and has swept to dominance from a frequency of <1% on 2025-07-02 to 99% in Europe as of 2025-11-21 [1]. This suggests a substantial fitness advantage over other J.2 viruses [2]. The combination of rapid growth, multiple antigenic substitutions in the haemagglutinin (HA) protein, antigenic mismatch with the vaccine strain, typically higher morbidity and mortality amongst the elderly during A/H3N2 seasons [3,4], and an unusually early start to the season have raised concerns over the potential for a severe season in the United Kingdom and Europe more broadly [5–7]. Furthermore, the 2025 flu season in Australia was one of the worst on record [8,9], and Japan is suffering from an early epidemic leading to school closures and increased hospitalisations [10]. These indicators suggest, though not definitively, an unusually severe influenza season ahead [11]. The interaction of season timing, antigenic drift, other subtype dynamics, vaccine efficacy and coverage, non-HA-mediated immunity, immune waning from previous seasons, climate factors, and contact pattern changes around school holidays is complex and leads to highly varied cumulative and peak seasonal burden [11,12]. The potential outlook of the 2025/26 influenza season is therefore uncertain, though historical seasons with early onset and peaks have often been severe [4].

One of the key concerns around clade K is that it has an estimated growth rate advantage of ~20% over competing strains based on clade frequency data. Multinomial logistic regression was used to estimate the relative fitness of clade K based on its coefficient in the regression model fitted to clade frequencies over time [2], giving an estimated selection coefficient of around 1.2. How this growth rate advantage translates to an estimate for the effective reproduction number R_e depends on the choice of reference strain and the R_e of that strain. A systematic review found that the median effective reproduction number for seasonal influenza was 1.28 (IQR: 1.19-1.37), with the estimated reproduction number in 2009 (pandemic H1N1) at 1.46 (IQR: 1.30-1.70) [13].

Real-time epidemiological assessment in England is based on weekly influenza surveillance data from the Second Generation Surveillance System (SGSS) [14]. SGSS compiles test results for infectious diseases including COVID-19, influenza, RSV and others from multiple data streams: the Royal College of General Practitioners Research & Surveillance Centre (primary care), the Respiratory DataMart system (hospital testing) and other hospital testing. The main surveillance indicator in the UK Health Security Agency weekly surveillance reports is the percentage of tests that are positive for influenza, out of those patients presenting with influenza-like illness (ILI). This metric has increased much earlier than in other recent seasons following the decline of a previous COVID-19 wave, particularly among the 5-14 year old age group. Note that Scotland, Wales and Northern Ireland have separate data reporting systems and have also recently reported substantial increases in influenza activity, though with a slight lag to England [15–17].

Despite its widespread use, metrics based solely on the percentage of tests positive for influenza are known to be biased by the dynamics of other ILI-causing pathogens which makes interpretation difficult. It is therefore recommended to use an ILI+ indicator which multiplies ILI cases by the percentage of tests positive for influenza, ideally stratified by subtype [18]. This metric can be generated from publicly available data sources from UKHSA. The WHO also provides a useful global data source for influenza dynamics in England, FluNet, which combines samples from non-sentinel (e.g., outbreak investigation, POC testing etc) and sentinel surveillance sites to give subtype-specific case counts over time [19]. We focus here on these sources of influenza case counts, either overall or by subtype, and stratified by age for recent years, to understand the

transmission rate of the current clade K viruses in the UK based on traditional measures of absolute growth rate and R_t.

In this report, we analyse publicly available epidemiological data from the UK and present modelling analyses using an age-stratified Susceptible-Infected-Recovered model to address two main questions:

1. Do the epidemiological data indicate a more transmissible A/H3N2 strain than previous seasons?
2. Under plausible scenarios of a virus with increased transmissibility, earlier seeding, and/or substantial immune evasion, what is the potential impact on cumulative and peak healthcare burden for the rest of the season?

To allow visualisation and exploration of different parameter combinations within the model runs and constructed analyses, we embedded our model into an interactive webtool using a service provided by shinyapps.io (https://www.shinyapps.io/). The tool (accessible at https://hay-idd.shinyapps.io/ModelFluUk-H3N2/) enables users to reproduce our results, but also allows exploration of different parameter combinations.

Results

The maximum growth rate of influenza A/H3N2 cases in the current season is slightly higher than in previous seasons

We calculated weekly exponential growth rates of cases from WHO FluNet, case counts in England from the Respiratory DataMart system, and an ILI+ indicator constructed from the Royal College of General Practitioners Research and Surveillance Centre data (**Figure S1-2**). We compared raw and modelled growth rates from the current influenza season to previous seasons, using both generalised additive models (GAMs) and a penalised spline model described by Eales et al. (**Figure 1A, Figure S3-S5**) [20].

Using data from WHO FluNet, and aligning the epidemic curves to the epidemic peak across different seasons, the 2025/26 season to date shows an earlier peak (epidemiological week 40 vs. 49, 49, and 47) and a faster A/H3N2 peak weekly growth rate (posterior means and 95% CrI: 0.680 [0.503-0.871] vs 0.0886 [-0.0577-0.238], 0.388 [0.264-0.515] and 0.592 [0.493-0.708]) compared to the 2024/25, 2023/24 and 2022/23 seasons (respectively) (**Figure 1B**). Model fits overlaid on the empirical growth rates are shown in **Figure S6**. We note that the choice of smoothing model is has a relatively large impact on the estimated growth rates due to the amount of noise in the data, and thus we present an alternative fit using a Gaussian random walk, noting that the peak estimated A/H3N2 growth rate for the current season is higher under this model (**Figure S7**). Similar relative trends were observed using the RCGP RSC data (**Figure S8**).

Comparing growth rates using all influenza cases (i.e., aggregating A/H3N2, A/H1N1pdm09, unsubtyped influenza A, and influenza B) suggests that the overall peak influenza growth rate is comparable to previous seasons (**Figure S9&S10**). The 2025/26 season to date has a peak on epidemiological week 40 compared to weeks 49, 49 and 49 in the 2024/25, 2023/24 and 2024/25 seasons respectively. The 2025/26 season a peak weekly growth rate for 'all influenza' of 0.482 (posterior mean; 95% CrI: 0.385-0.584) compared to 0.528 (0.476-0.582), 0.584 (0.526-0.647) and 0.548 (0.505-0.593) for the 2024/2025, 2023/2024 and 2022/2023 seasons (respectively). The dominant subtype from each prior season back to 2014/15 is shown in **Table 1**.
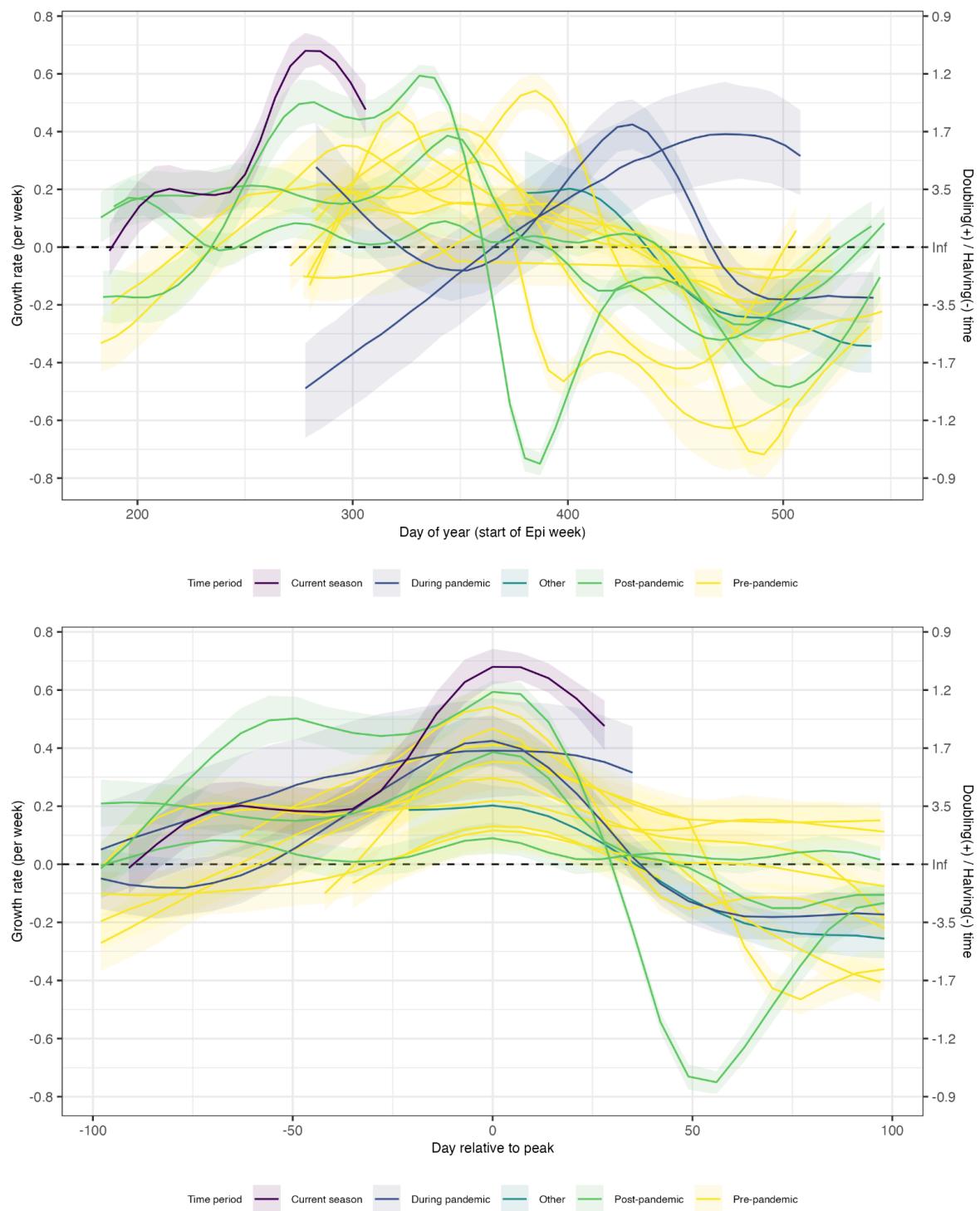
**Figure 1. Growth rate estimates of A/H3N2 cases from the WHO FluNet database using the penalised spline model**. Coloured lines and shaded regions show posterior mean and 95% credible intervals for the model-estimated weekly growth rate. Colouring distinguishes the current season from post, pre and during COVID-19 pandemic seasons. The doubling time corresponding to the growth rate is shown on the right hand y-axis.

Table 1. Summary of dominant influenza A subtypes by season (derived from UKHSA hospital typing data [21], Influenza | UKHSA data dashboard).

| Season	Dominant subtype
2014/15	A/H3N2
2015/16	A/H1N1pdm09
2016/17	A/H3N2
2017/18	A/H3N2
2018/19	A/H1N1pdm09
2019/20	A/H3N2
2020/21	N/A – COVID-19 pandemic
2021/22	A/H3N2
2022/23	A/H3N2
2023/24	A/H1N1pdm09
2024/25	A/H1N1pdm09
2025/26 (current)	A/H3N2
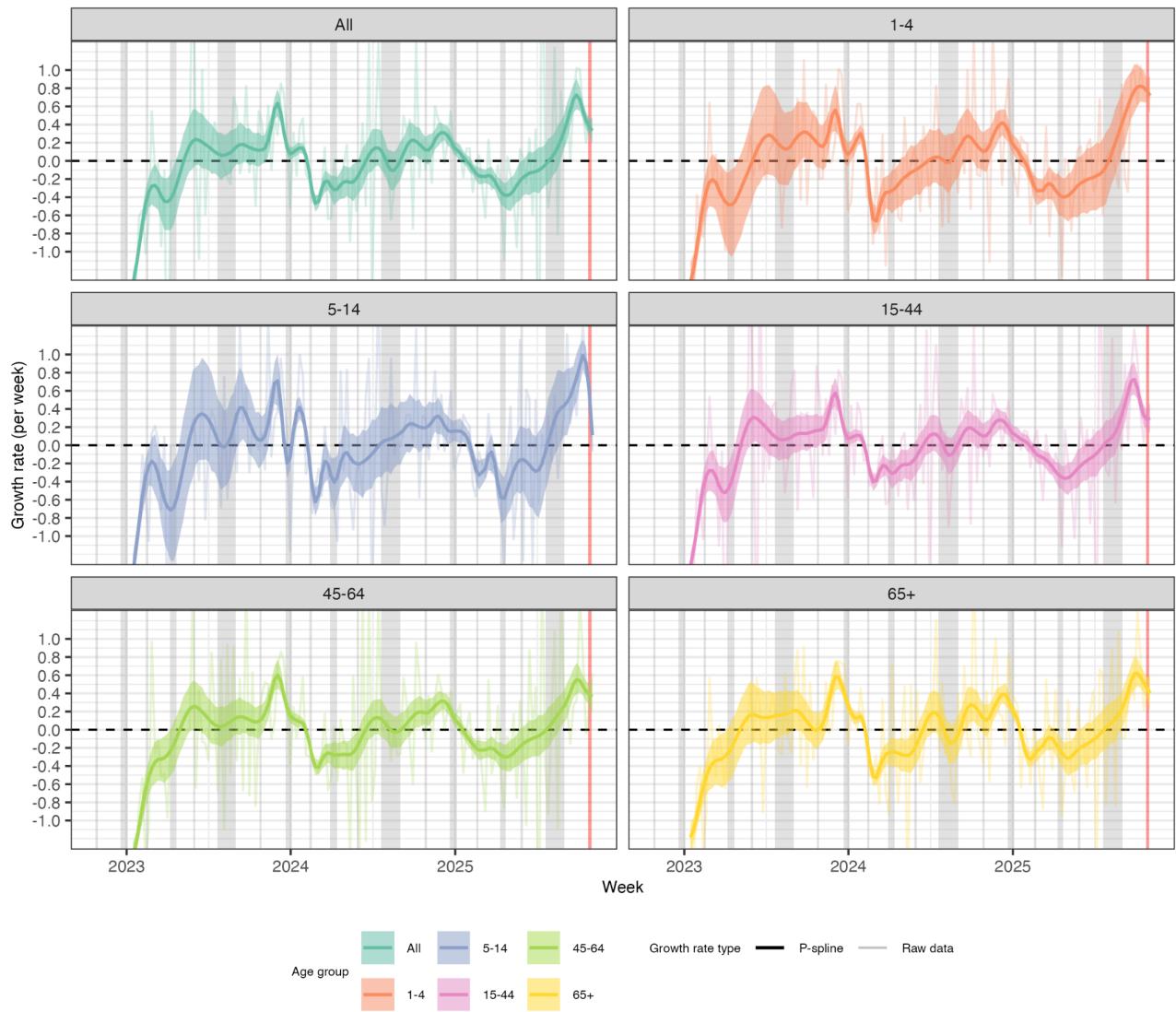
Figure 2. Growth rate estimates using a penalised spline model. School holidays are marked with vertical grey bars. The autumn half-term break in 2025 is marked in red. Solid lines and ribbons show posterior means and 95% credible intervals. We note that this is the date of the autumn half-term across most English schools, but there is a slight variation in some regions and schools Weekly log growth rates calculated directly from the data are shown in faint coloured lines to visually evaluate model fit.

Age-stratified growth rates highlight much higher growth in children than adults

We observed substantially higher recent growth rates of A/H3N2 cases in the 1-4 and 5-14 year old age groups compared to adults and adolescents (**Figure 2, Figure S11**). The difference in A/H3N2 weekly growth rates between children and the 15-44 year old age group was far higher than has been observed in the prior two influenza seasons (**Table 2**, **Figure S12**). A substantial drop in growth rates was observed preceding and during the recent Autumn half-term school break, consistent with previous years and with the known role of school contacts in driving influenza spread (**Figure 2**). However, we have so far only been able to obtain an age-stratified ILI+ indicator for A/H3N2 cases going back to the start of the 2023/2024 influenza season, which limits our ability to compare age-specific trends to previous A/H3N2 seasons. Comparison of these age-stratified growth rates to previous seasons should therefore be interpreted cautiously until historical data can be included.

Table 2. Values shown are the absolute difference in the posterior mean estimated peak weekly growth rate between the shown age group (years of age) and the 15-44 year old age group.

Season	1-4	5-14	45-64	65+
2023 to 2024	0.20	0.31	0.10	0.25
2024 to 2025	0.15	0.19	0.10	0.14
2025 to 2026	0.49	0.58	0.11	0.19

Estimates for the timevarying reproduction number suggest a similar peak infection rate to previous seasons

We used the WHO FluNet data from 2015 to 2025 to estimate the timevarying reproduction number, R_t. Note that here we distinguish R_t from the effective reproduction number, R_e, which we define as the reproduction number at the start of the season. Across the influenza seasons 2015/16, 2016/17, 2017/18, 2018/19, 2021/22, 2022/23, 2023/24, 2024/25, and 2025/26, the estimated time-varying reproduction number R_t generally remained close to 1, with intermittent fluctuations dropping below 1 and occasionally reaching values above 1.4 (**Figure 3**). When trajectories were aligned relative to the pre-Christmas period (before December 25), peak R_t values consistently occurred between early October and approximately December 20 across all seasons examined (**Figures 4, Figure S13**). Notably, post-COVID-19 pandemic seasons exhibited relatively stable R_t trajectories, and the 2025/26 season was in line with previous seasons, with R_t estimates not exceeding 1.4 (posterior mean; 95% credible intervals: 1.22, 1.47). This suggests that the overall dynamics for the most recent season (2025/26) were broadly similar to those of previous seasons.

For comparison we also estimated the current R_e in Japan, which at time of writing has been experiencing a longer period of exponential growth driven by clade K than England has. We obtained point estimates of 9.16 days for the doubling time and 1.26 for R_e.
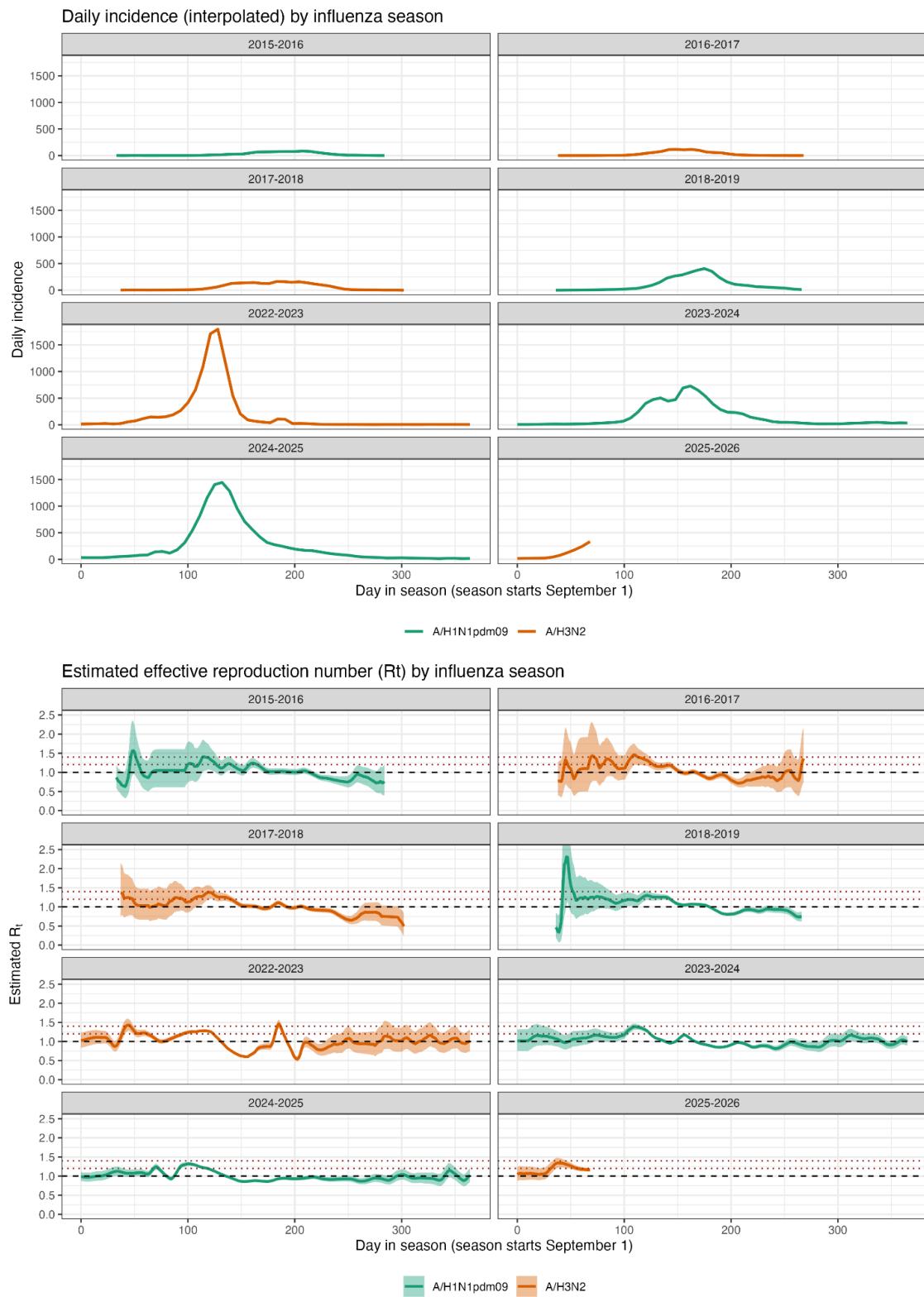
Figure 3: Top panel: Daily incidence combining all influenza subtypes for influenza seasons 2015-16, 2016-17, 2017-18, 2018-19, 2022-23, 2023-24, 2024-25, and 2025-26. The daily incidence curves were derived by smoothing the weekly case counts obtained from the WHO FluNet dashboard. **Bottom panel:** Estimated effective reproduction numbers for the same seasons using the data in the top panel with the EpiEstim R package. Horizontal dashed lines show R_t=1, 1.2 and 1.4 for reference. All lines are shaded by the dominant subtype that season as shown in **Table 1.**
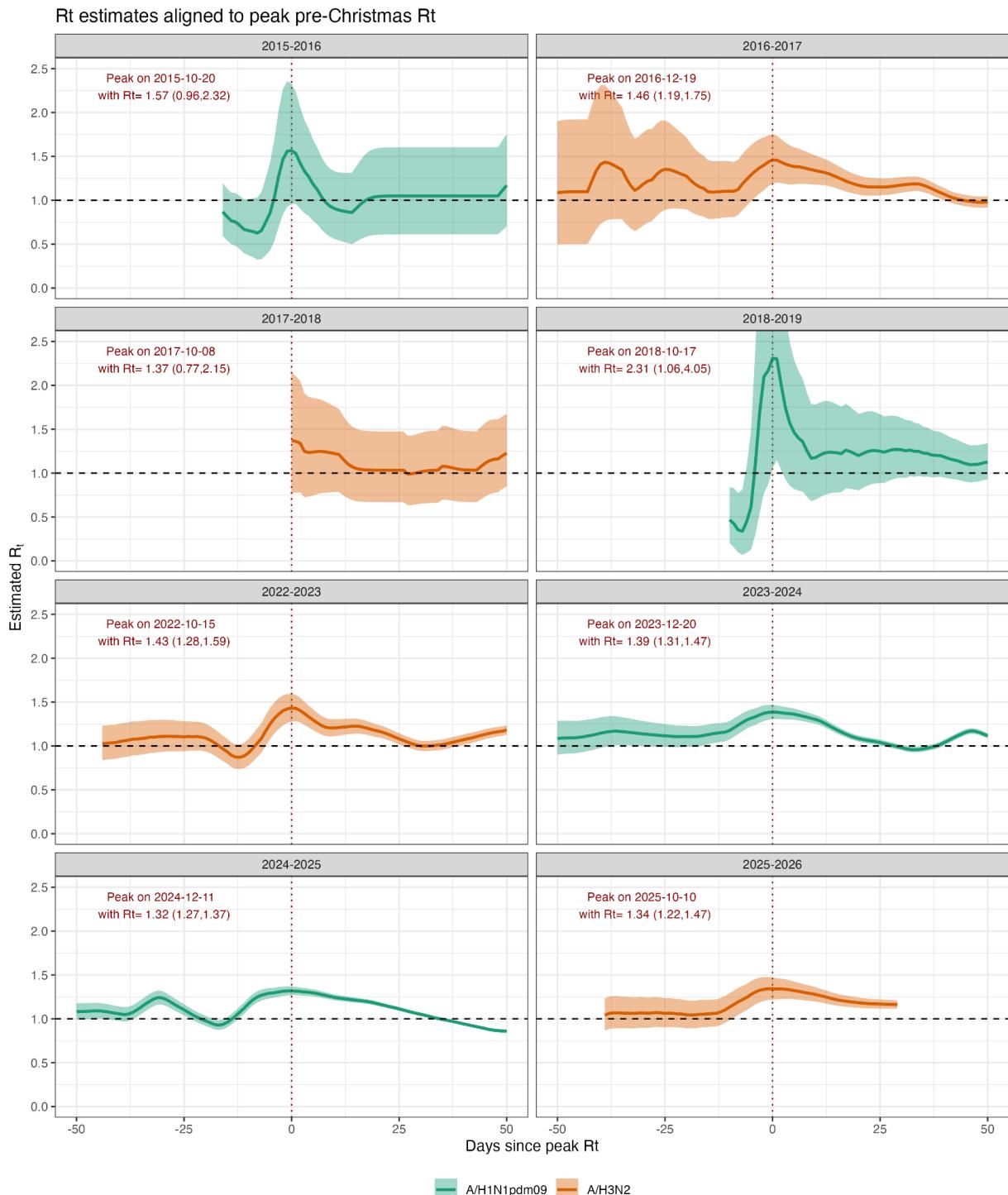
Figure 4: Effective reproduction number *(Rt)* for each influenza season arranged relative to peak pre-Christmas *Rt*. As in Figure 3, but aligning the curves to the date of peak *Rt* identified between June and before December 25 of that year. All seasons were aligned relative to their peak date by calculating the number of days since the peak. The date and estimated value of the peak *Rt* are shown in each subplot. Plots are coloured by their timing with respect to the COVID-19 pandemic. Note that we have excluded the COVID-19 pandemic years (2019/20 and 2020/21) where influenza activity was severely disrupted.

Scenario analyses using an age-stratified compartmental model

To explore potential scenarios distinguishing the current influenza season from the previous A/H3N2 season in 2022/23, we developed an age-stratified Susceptible-Infected-Recovered model and explored scenarios where the K clade viruses exhibit enhanced transmissibility, greater immune escape, or an earlier epidemic seed time. To allow visualisation and exploration of different parameter sets, we embedded the model's numerical code into an interactive webtool available at https://hay-idd.shinyapps.io/ModelFluUk-H3N2/.

Here we showcase some analysis using this webtool. The aim of this analysis was to understand if the unusually early influenza season might lead to unexpected epidemic dynamics as we enter the Christmas period when contact patterns change, and to test the impact of immune escape or increased transmissibility on overall disease burden. We also varied R_0, the overall proportion of the population immune to infection (as a proxy for immune escape), and the seed date of the epidemic to explore their impact on the final size, final size in 65+ year olds, and incidence at the peak as a proxy for maximum healthcare burden. All scenarios are shown in **Figure 5**, with dynamics in the 65+ age group shown in **Figure S14,** and the weekly growth rates of the scenarios are shown in **Figure S15**.

We include the modelled weekly growth rates of A/H3N2 cases from the first week of November for comparison in **Figure 5** using both the WHO FluNet and RCGP data. We note that although the two datasets give different estimates for the first week of November, they give almost identical estimates for the first week of October, suggesting that they capture broadly similar trends.

Moderate to severe immune escape results in larger epidemics with a pre-Christmas peak

Small reductions in the initial immune proportion had a drastic impact on the timing and overall burden of the epidemic (**Table 3; Figure 5&6, Figure S15**). Reducing the initial proportion of the population in the immune compartment by just 5% (relative to the compartment's size) led to an increase in the overall final size of the epidemic, with cases increasing much earlier in the season but still peaking in early December. Larger drops in initial population immunity quickly led to implausibly early and large epidemics, which is inconsistent with current surveillance data, suggesting that the level of immune escape of the K clade strain is likely to have reduced population immunity by no more than 10%. Scenarios with increased immunity escape lead to an earlier and larger epidemic that could peak in early December.

Drastically reducing the immune fraction only in individuals under 18 years of age also led to an implausibly large and early epidemic. More moderate reductions in immunity in children led to a much longer epidemic duration, but a similar total final size and lower peak. This is likely due to the interaction with the half term period, which acts as a temporary circuit break to dampen the incidence curve. A small increase in incidence following the half term is expected under this scenario.

Increased intrinsic transmissibility (proxied by increasing R_0 without changing the population immune fraction) led to an earlier epidemic peak and more cases prior to the Christmas period, though increasing R_0 from 2 to 2.5 did not appear to have a major impact on the overall final size (**Figure 6** top row). Again, this may be due to the timing of the half-term schools' holidays in England which dampens the growth rate. In both scenarios with R_0=2.2 and R_0=2.4, a drop in cases during half term followed by an increase would be expected.

Earlier season seeding results in a longer epidemic with reduced final size

Seeding the epidemic earlier led to a much more drawn out epidemic with a lower final size.
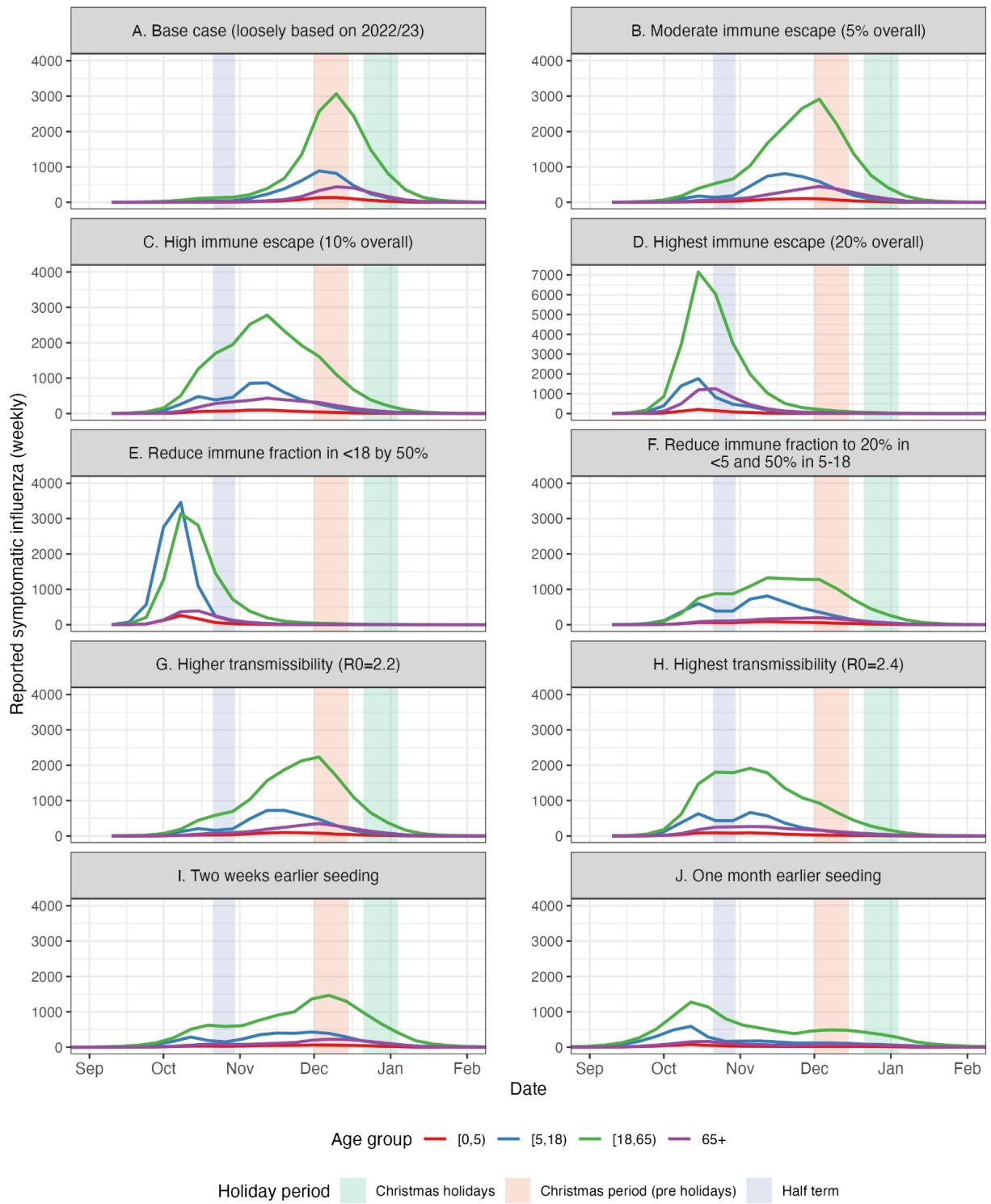
Figure 5. Comparison of epidemic trends across different model scenarios varying assumptions around the new A/H3N2 K clade immune escape, transmissibility and seed date. Note that the base case is based on loose visual fitting to the 2022/23 seasonal influenza case data from the RCGP surveillance centre. Dynamics in the 65+ age group only are shown in **Figure S14.** <u>This base scenario should be interpreted with caution as no formal fitting was performed, and thus there is considerable underrepresented uncertainty and risk of poor parameterisation.</u>

Table 3. Comparison of peak disease burden and overall disease burden of model scenarios relative to base case. All results shown are based on the ratio of outputs from the scenario to the base case. We do not report absolute numbers due to the lack of formal model fitting (other than the epidemic final size of the base case to roughly guide interpretation of the ratios).

| Scenario label	Scenario	Parameters changed from baseline	Peak of weekly symptomatic cases	Date of peak symptomatic cases	Cumulative symptomatic cases	Final size in 65+	Final size	Interpretation
A	Base case (loosely based on the 2022/23 season)	-	1.00	10/12/2022	1.00	1.00 (6.88%)	1.00 (18.7%)	Model parameters are roughly calibrated to match the 2022/23 influenza season, but we note that there is considerable hidden uncertainty, strong correlations between model parameters and structural identifiability issues.
B	Moderate immune escape	Immune escape parameter set to 0.95	0.91	03/12/2022	1.21	1.29	1.17	A relatively small loss of population immunity leads to a larger outbreak overall. The interaction with half term slightly lowers the peak incidence and the outbreak peaks before the Christmas holiday.
C	High immune escape	Immune escape parameter set to 0.9	0.94	12/11/2022	1.35	1.57	1.28	As in B, but with a much larger overall impact.
D	Severe immune escape	Immune escape parameter set to 0.8	2.32	15/10/2022	1.75	2.36	1.60	This can be ruled out, as an extremely large epidemic would have already peaked before half term.
E	Minor reduction in immunity in children	Initial immune fraction in 0-4 reduced to 20%; initial immune fraction in 5-18 reduced to 50%	0.54	12/11/2022	0.94	0.81	1.01	Dampens the peak due to the half term circuit break. Leads to similar overall final size and lower burden in older adults. A resurgence after half term is expected.
F	Severe reduction in immunity in children	All initial immune fractions in <18 year olds reduced by 50%	1.62	08/10/2022	1.01	0.69	1.14	An outsized impact on attack rates and peak burden in children, but a lower final size in older adults.
G	Higher transmissibility	$R0$ increased from 2 to 2.2	0.70	03/12/2022	1.06	1.07	1.05	Similar impact to B, with an earlier rise in cases dampened by half term leading to lower peak burden but higher overall incidence.
H	Severe transmissibility	$R0$ increased from 2 to 2.4	0.66	05/11/2022	1.04	1.06	1.04	Counterintuitively, leads to a much more drawn out epidemic with slightly lower incidence. This is likely due to the timing of the half term dampener with respect to incidence, which lessens the overshoot of infections after herd immunity is reached.
I	Two week earlier seeding	Seeding on 2025-08-24 rather than 2025-09-10	0.48	07/12/2022	0.87	0.85	0.88	An overall lower burden of infection and much lower beak burden, with a peak expected in early December.
J	One month earlier seeding	Seeding on 2025-08-01 rather than 2025-09-10	0.69	12/10/2022	0.99	0.66	0.75	Similar to I, but with an expected peak before half term.
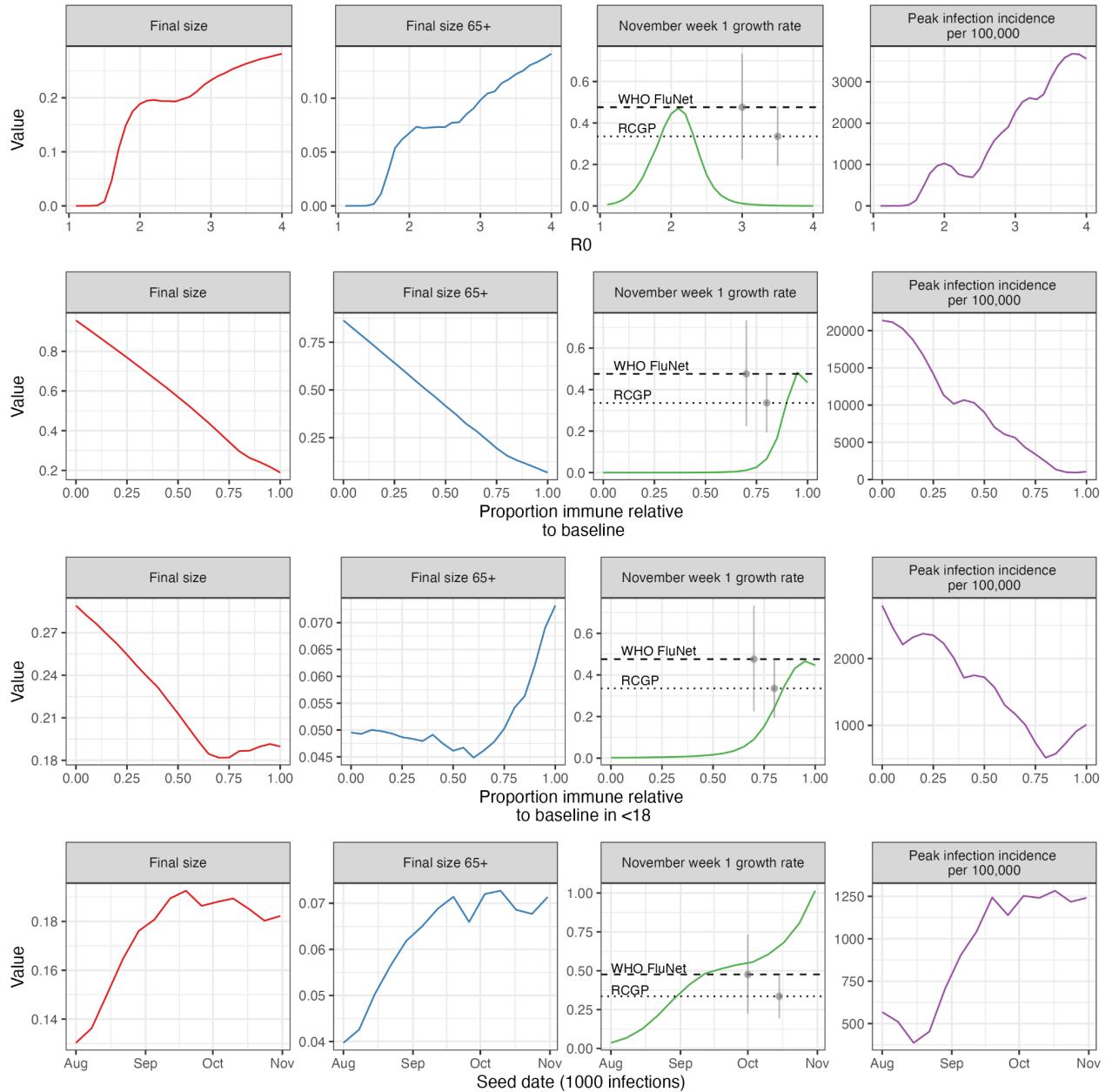
Figure 6. Univariable sensitivity analyses of the model outputs with respect to key parameters. Each row shows the impact of varying one parameter, given in the x-axis label, whilst keeping all other parameters at their baseline values. Results shown are for the epidemic final size (proportion of the population infected) overall and within the 65+ age group, the epidemic growth rate in the first week of November, and the peak weekly infection incidence. Note that the y-axes are different in each subplot. In the "November week 1 growth rate" plots, the horizontal dashed lines show the posterior mean estimated weekly epidemic growth rate in all age groups estimated using either the WHO FluNet data or the RCGP data. The grey pointrange plots show the 95% CrI. Note that the position of these pointrange plots on the x-axis is arbitrary – readers might use these pointrange plots to identify values on the x-axis which are compatible with observed growth rates.

Discussion

To better understand the burden of the influenza spread in England over the autumn and pre-Christmas period, we used the publicly available influenza data combined with an age-stratified transmission model embedded into a webtool that allowed us to explore different parameter scenarios.

Our analysis highlights that the currently spreading K clade of influenza in England has higher peak epidemic growth rates but similar effective reproduction numbers to those in previous severe seasons over the past 10 years. With the effective reproduction number peaking at around $R_t \sim 1.4$ (CI=[1.22,1.47]) based on current data, this is slightly higher than the typical R_e of seasonal influenza of 1.2-1.3 reported in the literature, but similar to what we estimated using the EpiEstim R package for previous seasons. This is also reflected in estimated peak growth rates so far, which are only slightly higher than previous peak levels. Notably, there have been substantially higher growth rates of A/H3N2 cases this season in children (ages 1-4 and 5-14 years old) compared to adults. We also ran scenario analyses to explore possible virus changes which might be compatible with the earlier start to the season. Only small reductions in population immunity due to immune escape are required to drive an earlier influenza season with more cumulative infections, but with a lower peak incidence, likely due to the half-term school holiday acting as a circuit breaker.

Overall, our findings suggest that the total infection burden is likely to be at the upper end of typical influenza seasons. High incidence can strain the health and healthcare systems in England, and preparedness plans should be made accordingly to avoid overwhelming hospitals in the coming weeks.

The influenza season, defined as weeks when ILI activity is above a baseline threshold [22], typically begins in November and peaks around the New Year each season, with cases reaching low levels by March [23]. However, it is not uncommon for the season to start and peak earlier or later [4]. The timing of the start of the season is likely affected by the volume of seeding of new infections from tropical and subtropical regions where influenza circulates year-round and that phylogenetic analysis has identified as the likely source of new variants [24]. Different patterns of travel to and from the UK could therefore explain the difference between the current UK epidemic to that seen in European neighbour countries that have not yet started their influenza season.

Notably the high epidemic of 1989/90 was driven by A/H3N2, characterised by an early peak in November with maximal incidence in children below the ages of 14 years old [4]. The historical experience of severe past seasons which began and peaked early warrants caution for the current season, and thus our findings should be interpreted in this context.

Recent influenza seasons cannot be easily compared to historic data, as influenza circulation and thus the accumulation of population immunity was severely disrupted by non-pharmaceutical interventions during the pandemic, with no activity during the 2020/21 season, and a very delayed 2021/22 season. Seasonal dynamics have since returned to near pre-pandemic patterns, but with a larger overall healthcare burden [21].

Immune escape from both the vaccine strain and the overall population immune landscape are thought to be key predictors of subsequent seasonal influenza burden. A pertinent analysis by Perofsky et al. [11] showed that genetic distance at epitope sites in H3 and N2 from previous seasonal strains, and a low local branching index of N2 (a low value suggests fewer, but more dominant strains) are predictors of season severity in the USA, though the correlation with

reduction in HI titre alone was not found to be significant [11]. They also noted earlier onset and peak timing for antigenically novel H3N2 viruses, but this trend was not statistically significant. For the clade K A/H3N2 viruses, substantially reduced reactivity of vaccine raised ferret antisera has been observed [5,25], and antigenic cartography placed K clade viruses at least 3 unit (8-fold reduction in HI titer) from the selected vaccine strain [26]. Neutralisation assays using human sera also suggested substantial antigenic advance, but to a lesser degree than suggested by the ferret sera [26]. Our analyses suggest that the effective level of immune escape at the population level (i.e. taking into account all components of immunity, not just humoral antibody responses) is relatively modest and comparable to previous seasonal influenza cluster transitions. We infer this from the fact that peak transmission rates are similar to those observed in past seasons, and from the scenario analyses, where even small reductions in initial population immunity were sufficient to reproduce the earlier onset and overall burden of the current season. Substantially greater immune escape would be expected to generate an even earlier start and markedly higher peak growth rates than those observed.

Vaccine efficacy against disease and hospitalisation is also an important factor for projecting seasonal burden, though efficacy against disease is often fairly low (compared to other vaccine preventable diseases) even in years where the vaccine strain is well matched. A recent meta analysis found that influenza vaccination had a pooled vaccine effectiveness of 48% (95% CI, 39 to 55) in adults between the ages of 18 and 64 years and 67% (95% CI, 58 to 75) in children against hospitalisation [27]. Based on test negative design data (i.e., VE against laboratory-confirmed symptomatic infection), A/H3N2 VE for the 2024/25 season ranged between 29-47% among all ages in primary care settings, with lower VE in adults and higher VE in children, noting that different age groups are recommended different vaccines [28]. Preliminary vaccine effectiveness data from England for the 2025/26 season are reassuring, estimating 70-75% VE in children and 30-40% VE in adults against hospitalisation [5]. However, these results are early and based on small sample sizes. Continued monitoring of vaccine efficacy over the season is recommended, and an improved understanding of how antigenic escape measured on antibody assays predicts loss of VE is needed.

In addition to virus and immunological factors, seasonal forcing is known to be crucial in initiating the annual influenza season in the northern hemisphere when paired with the increase in population mixing at the start of the school year in September [29–32]. The timing of the seeding of the K clade in England, the drop in absolute humidity going into autumn, and the start of the school term in September may have led to earlier seeding than some previous seasons. We did not analyse the role of absolute humidity in the start of the 2025/26 influenza season in England, but crude exploratory analyses (not shown) and assessment of the literature suggest that a small drop in absolute humidity in the coming months would at most contribute to a 5-10% increase in transmission rates. The depletion of susceptibles and role of within-school mixing and school term timing likely have a much larger role and thus we do not anticipate substantially higher transmission rates going forward from climate factors alone.

Contact patterns change considerably over time with consequences for transmission rates. For seasonal influenza, which is likely driven by high within-age-group social mixing and greater susceptibility to infection in children, school term times and holidays can have a major impact on the shape of the epidemic [31]. In our scenario analyses, we modelled school holidays and the Christmas period in early December by scaling contact rates in different settings based on recent analyses from digital contact tracing [33]. Although these changes are difficult to parameterise and can vary from year to year, our chosen scenarios likely represent realistic shifts in behaviour for the coming months. Whether a new strain with enhanced transmissibility or immune escape will lead to a higher winter burden partially depends on the timing of peak transmission relative to school

holidays – the half-term holiday can act as a circuit breaker, dampening the peak and spreading cases over a longer period of time. All of our scenarios place peak incidence prior to the Christmas holiday when increased mixing across age groups is expected, reducing the opportunity for transmission into older individuals.

This work presented here aims to make two contributions to situational awareness. First, we aimed to address two key unknowns early in the influenza season in England: 1) whether early epidemiological data are consistent with predictions from immunological and genomic data; and 2) identifying the range of potential epidemic dynamics compatible with current incidence trends. These types of analyses were used widely during the COVID-19 pandemic [34,35], but have since become less common for seasonal respiratory diseases. The analyses performed here are relatively straightforward and quick, using data which are already routinely collected. Second, to understand and support the model outcomes, we have set out to design an interactive visualisation tool that we made available online. Given that the model has a large number of parameters, a large number of scenario analysis can be explored. Devising a compact visualisation tool to capture the possibility of different model outcomes allows users to explore scenarios of interest that can enable insights to be drawn on possible preparedness measures and inform policymakers of different response options.

Regular updating of data analyses of respiratory virus dynamics would achieve three benefits: improvements of data flows and schemas; improvements of analytical methods; and most importantly, easy contextualisation of sudden change, such as the appearance of the current K strain of influenza. For understanding the significance of such changes to health and health systems, systems and decision making tools such as the Shiny app presented here should be maintained regularly and updated early in the season to rule in or out different scenarios. Maintaining the toolkit shown here requires low-resource but consistent input from technical specialists, and real-time access to absolute reported case numbers rather than just percentage of tests positive for influenza.

Our analyses have a number of limitations, some due to limitations in data, and some due to the rapid nature of our analysis. For the epidemiological analyses, we combined data from multiple sources (UKHSA reports, RCGP RSC, WHO FluNet, Respiratory DataMart). These data sources each have their own limitations in representativeness and reporting algorithms [36], and our analyses required additional assumptions to align age groups and dates. Growth rate and R_t estimates are also possibly biased by changes in testing intensity and reporting rates between age groups. When estimating growth rates, we used a penalised spline model to smooth the incidence curve, which may mask true sudden changes in growth rates. For the R_t analyses, we used WHO FluNet non-sentinel surveillance data, which also have caveats around representativeness and testing intensity, and used all influenza positive samples, which will mask subtype-specific transmission rates. We also smoothed the incidence data to help with model convergence, which again might mask genuine fluctuations in transmission rates. We also note that overconfident estimates from small sample sizes are a known issue with EpiEstim. All of the data used were reported weekly, which might obscure model finely resolved effects. Direct access to the UKHSA and RSGP influenza data would have potentially given us a more granular dataset, and if this were available in future, our analyses can be easily repeated.

The model used for scenario analyses is also heavily caveated, as we did not perform a formal model fit due to time constraints. Instead, we chose fixed parameter values based on commonly assumed influenza parameters (R_0, infectious period, final size), and then manually calibrated other parameters (e.g., reporting rates, age-specific symptomatic fraction, seed date and size) to achieve a reasonable visual fit to the 2022/23 influenza incidence data. Assumptions regarding

age-specific immunity, immune escape, and all-or-nothing immunity in two classes rather than stratified immunity ([37]) all have a large impact on the projected incidence curves, and we therefore recommend using the tool to inform a general understanding of the system rather than predictions. A key omission is vaccination, which we did not include due to severe challenges in parameterising age-specific vaccine efficacy against infection and disease. The potential interaction of the early season with the time taken to achieve high vaccine coverage in high risk populations may be important. Our model is also limited by the use of outdated contact data, and also strong assumptions surrounding behaviour changes in school holidays and the Christmas period. Although we are confident that these assumptions capture general trends, more recent and well-calibrated parameter values would likely result in different epidemic trends.

It is important to note that in this report we have only considered data from England. Scotland, Wales and Northern Ireland have all experienced a later start to the influenza season, and thus our scenarios with half-term acting as a circuit breaker may be less relevant since the timing of half-term dates differ between the four UK nations. Furthermore, a later start to the season with moderate immune escape or increased transmissibility may result in much higher incidence during the Christmas period, which may translate into higher burden in the elderly. Within the visualisation interactive tool, users can upload alternative datasets and change the population size as well as alter different model parameters to create the scenario analyses. Hence it is possible to explore additional scenarios to understand possible dynamics in Scotland, Wales and Northern Ireland, which will be important to explore in the future through collaboration with policymakers in these nations.

In summary, we have combined publicly available influenza data for England with an age-stratified Susceptible-Infected-Recovered model and an interactive visualisation webtool. Our analysis shows that compared to previous years, the epidemic growth rate is high but not exceptional. Modelling analysis suggests that the epidemic trajectory so far is consistent with at most modest reduction in population immunity compared to previous years. Increases in transmission do not always translate to bigger epidemics because of the interaction between epidemic dynamics and school holidays. We provide a range of scenarios and an interactive scenario-explorer app, that show the impact of different assumptions on the epidemic curve for the coming months.

Methods

Epidemiological analyses

Data summary

The ideal dataset for understanding influenza epidemiological trends would be an unbiased measure of symptomatic A/H3N2 infection incidence stratified by age. However, it is not possible to obtain this exact dataset due to biases in testing behaviour and coverage, limitations of data reporting, and restrictions on public sharing. Instead, influenza surveillance in England consists of multiple indicators from different sources, ranging from primary care through to emergency department visits. Following recommendations from [18], our main aim was to develop an ILI+ indicator for each age group of interest, calculated as:

$$ILI_+ = ILI * p_{+ve} * p_{A/H3N2}$$

Where p_{+ve} is the proportion of all tests done which are positive for influenza and $p_{A/H3N2}$ is the proportion of all positive influenza tests which are attributed to A/H3N2.

In the time frame of this analysis, we were unable to construct one consistent dataset to use in all analyses and we therefore pieced together different data sets to generate as close to an ILI+ indicator by age as possible. We intend for future iterations of this analysis to simplify this process.

In brief, we used data on influenza cases by age group from the Royal College of General Practitioners (RCGP) Research & Surveillance Centre (RSC), data on ILI from the Respiratory DataMart system, and data for the percentage of influenza cases positive for A/H3N2 influenza from the Second-Generation Surveillance System (SGSS) (**Figure S1**). We multiplied these datasets together to obtain: 1) an ILI+ indicator by age group going back to 2023; 2) an estimate of absolute influenza cases (all subtypes) over time going back to 2009; 3) and an an estimate of age-stratified influenza cases (all subtypes) for the 2022/23 season (**see:** https://hay-idd.shinyapps.io/ModelFluUk-H3N2/). Further details on data processing are provided in the **Supplementary Material.**

As a comparator dataset, we also obtained weekly counts of reported influenza specimens stratified by subtype obtained from the WHO FluNet platform [19]. All data used are aggregated weekly and we used the final date of the epidemiological week as the reported date.

For the calculation of R_e for Japan, we used weekly cases counts reported at https://weathernews.jp/news/202511/210136/ extracted on 24/11/2025 (values translated as "The number of reports from fixed-point medical institutions over the past week"). We included values reported as being from 28/09/2025 (before which growth appeared sub-exponential) until 16/11/2025 (the latest available) inclusive. We took the generation time distribution to be gamma distributed with the mean and standard deviation reported in (Chan et al. 2024): 3.2 days and 2.1 days respectively.

Weekly growth rate calculations

Weekly growth rates were calculated for each influenza season and aligned by calendar week as:

$$y = log(\frac{i(t)}{i(t-1)})$$

Where $i(t)$ is the reported incidence over week t. We then produced smoothed weekly growth rate curves using two methods:

1. Fitting a penalised smoothing spline model to reported incidence data using the Bayesian method described by Eales et al [20]. We used the EpiStrainDynamics package using penalised splines with degree 3 and 3 weeks per knot [38]. We found that the model was unstable with low case counts, and thus for age-stratified growth rate estimates we first artificially inflated the counts 10-fold before fitting the model. Thus, uncertainty is likely unrepresented.
2. Fitting a Generalised Additive Model (GAM) using the *mgcv* R package predicting log weekly growth rate as a function of time, placing a penalised smoothing spline a basis dimension of up to 5 [39].

Time-varying reproduction number estimation

We estimated the time-varying effective reproduction number (R_t) using the *EpiEstim* package in R, which implements the method described by Cori et al. [40]. We used the overall weekly influenza incidence data for the period 2015–2025 from the WHO FluNet database for this analysis. To approximate daily incidence, weekly counts were disaggregated by distributing the cases evenly across days per week, followed by application of a 14-day rolling mean to smooth short-term fluctuations.

The serial interval distribution was assumed to follow a distribution with a mean of 3.6 days and a standard deviation of 1.6 days, based on [41]. R_t was computed over sliding weekly windows to capture temporal variation in transmission potential. The resulting R_t trajectories were visualised to compare epidemic dynamics across seasons, highlighting differences in transmissibility and potential shifts in seasonal patterns over the study period. In this analysis, we assumed that a typical flu season starts on September 1st each year.

For the estimation of R_e for Japan, we first estimated the exponential growth rate r using a simple linear regression model of log(cases) against date reported. We then estimated R_e using the relationship $R_e = 1 / \int_0^\infty \omega(\tau) e^{-r\tau} d\tau$ implied by the renewal equation [42].

Compartmental model and scenario analyses

Model overview

We simulated seasonal influenza transmission dynamics for England using an age- and immunity-structured deterministic Susceptible-Infected-Recovered model. We divided the population into four age groups (0-4, 5-18, 19-64 and 65+ years; Note that infants under 1 year were excluded, as we did not have age-stratified A/H3N2 ILI+ data for this age group) and two immunity classes (fully susceptible and partially immune). Contact rates within and between age groups were derived from the POLYMOD study using the *socialmixr* R package [43,44]. To account for changes in contact rates outside of school terms, we resampled from the original POLYMOD data to scale contact rates during the half term holiday, pre-Christmas period, and the Christmas school holidays (described below). For each age group, we tracked the overall incidence of infections, symptomatic cases and infections per week. We informally calibrated the model to reported overall influenza case data from the 2022/23 season to provide a baseline, and performed scenario analyses varying key model parameters to generate plausible scenarios for the 2025/26 season.

Model structure

The force of infection in group *i* was defined as:

$$\lambda_i(t) = \beta \sum_{j=1}^{m} C_{i,j}(t)I_j(t)$$

Where β is the overall transmission rate (not age-stratified), $C_{i,j}$ is the contact rate between group *i* and group *j*, and I_j is the number of infected individuals in group *j* at time *t*.

Transition rates between the three compartments were defined by the following set of ordinary differential equations:

$$\frac{dS_{a,k}}{dt} = -\alpha_k S_{a,k}(t)\lambda_{a,k}(t)$$

$$\frac{dI_{a,k}}{dt} = \alpha_k S_{a,k}(t)\lambda_{a,k}(t) - \frac{I_{a,k}(t)}{T_g}$$

$$\frac{dR_{a,k}}{dt} = \frac{I_{a,k}(t)}{T_g}$$

Where α_k denotes the relative susceptibility of immune class *k* and T_g is the infectious period. Note that α_k was set to 0 for the immune population, representing all-or-nothing immunity. Leaky immunity ($\alpha_k > 0$) leads to very dynamics. We solved the model in daily timesteps using the *deSolve* R package [45].

Immunity, initial conditions and seeding

We set the population size of the model to 60,000,000, corresponding to the population size of England. We distributed the population into age groups based on the age distributions returned by the *socialmixr* package using the POLYMOD data. Each age group was then stratified into the susceptible or fully immune class using varying proportions to capture different levels of immune escape for particular age groups. An additional immune escape multiplier, δ, was introduced to scale the overall population immune proportion (δ=0 corresponds to complete immune escape, whereas δ=1 corresponds to no loss of population immunity).

The epidemic was seeded by setting $I_a'(0) = s$ and $S_a'(0) = S_a(0) - s$, where *s* is the initial seed size and $S_a(0)$ is the number of individuals of age group *a* who are initially susceptible. Note that it is possible to vary the seed size, date and age group. We kept seeding in the youngest age group at 1000 initial infections in all scenarios, varying only the initial seed size.

Contact matrices over time

Base contact matrices were calculated from the POLYMOD UK data aggregated to the four age groups (0 to 5, 5 to 18, 18 to 65 and 65+ years). We generated four contact matrices for different periods of time: 1) regular school term-time; 2) half-term with no school contacts and reduced school contacts; 3) pre-Christmas shopping period (1-15 December) with an overall increase in non-school contacts; and 4) the Christmas school holiday period with no school contacts, a reduction in all contacts, and a substantial increase in at-home contacts. These four matrices were constructed by resampling the original POLYMOD contact diary entry data from the *socialmixr* R package with replacement and applying multipliers for home, work and other contact types. Holiday dates were based on the Oxfordshire school holiday period, though we note that holiday dates vary

over the country, and even more so over the UK. For all non-school contacts, the relative changes in contacts over half-term holidays and the Christmas period (shopping and holiday) were extrapolated from 2021-2023 data from Kendall et al. Science 2024 (see Figures 5A and 7B in the paper) [33]. Absolute changes in overall non-school contact rates were extrapolated from the same source (see Figures 1A, 7A in the paper).

To transition between these four different contact matrices, we generated a single contact matrix for each day, taking a weighted average of the four matrices depending on the time. For example, contacts in the middle of the school term were entirely governed by the term-time matrix (weighting of 1, all other matrices weighting 0), whereas contacts in the middle of the Christmas school holiday were governed entirely by the Christmas school holiday matrix. To ensure smooth transitions between these contact patterns, we smoothed the transition of weightings over 7 days before and after the holiday period using a cosine function.

Baseline model calibration

Model parameters were chosen based on standard seasonal influenza parameter values (R_0 of 2, infectious period of 4-5 days, and final size of around 15% [46]), intuition and manual calibration to generate seasonal dynamics similar to what was seen in the 2022/23 season. We note that this is a complex model with a large number of parameters, making formal model fitting extremely difficult. Some of the parameters are hard to identify and interpret, such as the overall fraction of symptomatic cases reported, the symptomatic fraction by age combined with age-specific reporting rates, and the level of immune escape of the seed virus. Parameter values used for the baseline scenario are shown in **Table 4**.

Scenario analyses

Scenario analyses were chosen to illustrate potential hypotheses for the early and rapid growth of A/H3N2 cases in England for the 2025/26 season. We also varied the immune escape scaling parameter δ, the basic reproduction number R_0, the proportion of the 0-4 and 5-18 year old population initially immune, and the seed date were varied invariably to generate **Figure 6**.

Implementation

All analyses were implemented and run in R version 4.2.2. The compartmental model was also implemented as a Shiny app with user-friendly sliders to change key parameter values, available at: https://hay-idd.shinyapps.io/ModelFluUk-H3N2/.

Table 4. Model parameters assumed for the baseline scenario. These are the default parameters in the interactive web tool.

Parameter	Assumed value
R_0: basic reproduction number	2
T_g: infectious period	4 days
γ: immune escape multiplier	1
Seed date	10th September
Seed size in age group 1 (0-4 yrs)	1000
Population size	60,000,000
Proportion of work contacts kept in school holidays	0.75
Multiplier for home contacts in school breaks	1
Multiplier for non-school and non-work contacts in school breaks	1.1
Multiplier for all non-school contacts in Christmas period (1-15 December)	1.3
Proportion of all contacts kept over Christmas	0.67
Multiplier for home contacts over Christmas holiday	3
Proportion initially immune (0-4 yrs)	0.3
Proportion initially immune (5-18 yrs)	0.6
Proportion initially immune (19-64 yrs)	0.7
Proportion initially immune (65+ yrs)	0.75
Symptomatic fraction and reporting rate (0-4 yrs)	0.05
Symptomatic fraction and reporting rate (5-18 yrs)	0.2
Symptomatic fraction and reporting rate (19-64 yrs)	0.35
Symptomatic fraction and reporting rate (65+ yrs)	0.45

References

1. auspice. [cited 19 Nov 2025]. Available: https://nextstrain.org/seasonal-flu/h3n2/ha/2y?dmin=2024-11-29&p=grid

2. Huddleston J, Chang J, Lee J, Steinberg P, Neher R, Bedford T. Seasonal influenza circulation patterns and projections for September 2025 to September 2026. Zenodo; 2025. doi:10.5281/ZENODO.17281059

3. Allen JD, Ross TM. H3N2 influenza viruses in humans: Viral mechanisms, evolution, and evaluation. Hum Vaccin Immunother. 2018;14: 1840–1847.

4. Fleming DM, Elliot AJ. Lessons from 40 years' surveillance of influenza in England and Wales. Epidemiol Infect. 2008;136: 866–875.

5. Kirsebom FCM, Thompson C, Talts T, Kele B, Whitaker HJ, Aziz NA, et al. Early influenza virus characterisation and vaccine effectiveness in England in autumn 2025, a period dominated by influenza A(H3N2) subclade K. 2025. Available: https://assets.publishing.service.gov.uk/media/691349457a0ccd6a3aad7fa9/_Flu_interimVE_2526_.pdf

6. Iacobucci G. Flu in numbers: NHS faces one of worst winters ever, officials warn, amid concern over mutated strain. BMJ. 2025;391: r2391.

7. European Centre for Disease Prevention and Control. Threat Assessment Brief - Assessing the risk of influenza for the EU/EEA in the context of increasing circulation of A(H3N2) subclade K - 20. ECDC. 2025.

8. Dashboard · NINDSS Portal. [cited 18 Nov 2025]. Available: https://nindss.health.gov.au/pbi-dashboard/

9. Australia posts record-breaking flu numbers as vaccination rates stall. [cited 18 Nov 2025]. Available: https://www.racgp.org.au/gp-news/media-releases/2025-media-releases/october-2025/australia-posts-record-breaking-flu-numbers-as-vac

10. Fieldhouse R. Japan declares a flu epidemic - what this means for other nations. Nature. 2025 [cited 18 Nov 2025]. doi:10.1038/d41586-025-03367-z

11. Perofsky AC, Huddleston J, Hansen C, Barnes JR, Rowe T, Xu X, et al. Antigenic drift and subtype interference shape A(H3N2) epidemic dynamics in the United States. 2024. doi:10.7554/elife.91849.1

12. Dalziel BD, Kissler S, Gog JR, Viboud C, Bjørnstad ON, Metcalf CJE, et al. Urbanization and humidity shape the intensity of influenza epidemics in U.S. cities. Science. 2018;362: 75–79.

13. Biggerstaff M, Cauchemez S, Reed C, Gambhir M, Finelli L. Estimates of the reproduction number for seasonal, pandemic, and zoonotic influenza: a systematic review of the literature. BMC Infect Dis. 2014;14: 480.

14. UK Health Security Agency. National flu and COVID-19 surveillance reports: 2025 to 2026 season. GOV.UK; 2025. Available: https://www.gov.uk/government/statistics/national-flu-and-covid-19-surveillance-reports-2025-to-2026-season

15. Weekly Influenza and Acute Respiratory Infection Report. In: Public Health Wales [Internet]. [cited 20 Nov 2025]. Available: https://phw.nhs.wales/topics/immunisation-and-vaccines/fluvaccine/weekly-influenza-and-acute-respiratory-infection-report/

16. Public Health Scotland. Influenza. [cited 20 Nov 2025]. Available: https://publichealthscotland.scot/population-health/health-protection/infectious-diseases/influenza/data-and-surveillance/

17. Respiratory surveillance report. 12 Nov 2025 [cited 20 Nov 2025]. Available: https://www.publichealth.hscni.net/services-and-teams/public-health-services/health-protection/surveillance-data/respiratory-0

18. Eales O, McCaw JM, Shearer FM. Biases in routine influenza surveillance indicators used to monitor infection incidence and recommendations for improvement. Influenza Other Respi Viruses. 2024;18: e70050.

19. flunetchart. [cited 7 Nov 2025]. Available: https://worldhealthorg.shinyapps.io/flunetchart/

20. Eales O, Windecker SM, McCaw JM, Shearer FM. Inferring temporal trends of multiple pathogens, variants, subtypes or serotypes from routine surveillance data. Am J Epidemiol. 2025; kwaf119.

21. UKHSA data dashboard. [cited 24 Nov 2025]. Available: https://ukhsa-dashboard.data.gov.uk/respiratory-viruses/influenza

22. Vega T, Lozano JE, Meerhoff T, Snacken R, Mott J, Ortiz de Lejarazu R, et al. Influenza surveillance in Europe: establishing epidemic thresholds by the moving epidemic method. Influenza Other Respi Viruses. 2013;7: 546–558.

23. Timing of influenza seasons. In: GOV.UK [Internet]. 28 Nov 2022 [cited 23 Nov 2025]. Available: https://www.gov.uk/government/publications/respiratory-virus-circulation-england-and-wales/timing-of-influenza-seasons

24. Bedford T, Riley S, Barr IG, Broor S, Chadha M, Cox NJ, et al. Global circulation patterns of seasonal influenza viruses vary with antigenic drift. Nature. 2015;523: 217–220.

25. Sabaiduc S, Kaweski SE, Separovic L, Gao R, Ranadheera C, Bastien N, et al. Emergence of seasonal influenza A(H3N2) variants with immune escape potential warrants enhanced molecular and epidemiological surveillance for the 2025–2026 season. Journal of the Association of Medical Microbiology and Infectious Disease Canada. 2025. doi:10.3138/jammi-2025-0025

26. Kikawa C, Huddleston J, Loes AN, Turner SA, Lee J, Barr IG, et al. Near real-time data on the human neutralizing antibody landscape to influenza virus to inform vaccine-strain selection in September 2025. bioRxivorg. 2025. doi:10.1101/2025.09.06.674661

27. Scott J, Abers MS, Marwah HK, McCann NC, Meyerowitz EA, Richterman A, et al. Updated evidence for Covid-19, RSV, and influenza vaccines for 2025-2026. N Engl J Med. 2025. doi:10.1056/NEJMsa2514268

28. Rose AM, Lucaccioni H, Marsh K, Kirsebom F, Whitaker H, Emborg H-D, et al. Interim 2024/25 influenza vaccine effectiveness: eight European studies, September 2024 to January 2025. Euro Surveill. 2025;30. doi:10.2807/1560-7917.ES.2025.30.7.2500102

29. te Beest DE, van Boven M, Hooiveld M, van den Dool C, Wallinga J. Driving factors of influenza transmission in the Netherlands. Am J Epidemiol. 2013;178: 1469–1477.

30. Shaman J, Pitzer VE, Viboud C, Grenfell BT, Lipsitch M. Absolute humidity and the seasonal onset of influenza in the continental United States. PLoS Biol. 2010;8: e1000316.

31. Cauchemez S, Valleron A-J, Boëlle P-Y, Flahault A, Ferguson NM. Estimating the impact of school closure on influenza transmission from Sentinel data. Nature. 2008;452: 750–754.

32. van Noort SP, Águas R, Ballesteros S, Gomes MGM. The role of weather on the relation between influenza and influenza-like illness. J Theor Biol. 2012;298: 131–137.

33. Kendall M, Ferretti L, Wymant C, Tsallis D, Petrie J, Di Francia A, et al. Drivers of epidemic dynamics in real time from daily digital COVID-19 measurements. Science. 2024;385: eadm8103.

34. Howerton E, Contamin L, Mullany LC, Qin M, Reich NG, Bents S, et al. Evaluation of the US COVID-19 Scenario Modeling Hub for informing pandemic response under uncertainty. Nat Commun. 2023;14: 7260.

35. Abbott S, Hellewell J, Thompson RN, Sherratt K, Gibbs HP, Bosse NI, et al. Estimating the time-varying reproduction number of SARS-CoV-2 using national and subnational case counts. Wellcome Open Res. 2020;5: 112.

36. Data quality report: national flu and COVID-19 surveillance report. In: GOV.UK [Internet]. [cited 22 Nov 2025]. Available: https://www.gov.uk/government/publications/sources-of-surveillance-data-for-influenza-covid-19-and-other-respiratory-viruses/data-quality-report-national-flu-and-covid-19-surveillance-report#about-this-report

37. Yuan H-Y, Baguelin M, Kwok KO, Arinaminpathy N, van Leeuwen E, Riley S. The impact of stratified immunity on the transmission dynamics of influenza. Epidemics. 2017;20: 84–93.

38. EpiStrainDynamics. Github; Available: https://github.com/acefa-hubs/EpiStrainDynamics

39. Wood S. Mixed GAM Computation Vehicle with Automatic Smoothness Estimation [R package mgcv version 1.9-4]. In: Comprehensive R Archive Network (CRAN) [Internet]. 7 Nov 2025 [cited 22 Nov 2025]. Available: https://cran.r-project.org/web/packages/mgcv/index.html

40. Cori A, Ferguson NM, Fraser C, Cauchemez S. A new framework and software to estimate time-varying reproduction numbers during epidemics. Am J Epidemiol. 2013;178: 1505–1512.

41. Cowling BJ, Fang VJ, Riley S, Malik Peiris JS, Leung GM. Estimation of the serial interval of influenza. Epidemiology. 2009;20: 344–347.

42. Wallinga J, Lipsitch M. How generation intervals shape the relationship between growth rates and reproductive numbers. Proc Biol Sci. 2007;274: 599–604.

43. Social Mixing Matrices for Infectious Disease Modelling [R package socialmixr version 0.4.0]. In: Comprehensive R Archive Network (CRAN) [Internet]. 18 Oct 2024 [cited 22 Nov 2025]. Available: https://cran.r-project.org/web/packages/socialmixr/

44. Mossong J, Hens N, Jit M, Beutels P, Auranen K, Mikolajczyk R, et al. Social Contacts and Mixing Patterns Relevant to the Spread of Infectious Diseases. Riley S, editor. PLoS Med. 2008;5: e74.

45. Solvers for Initial Value Problems of Differential Equations ('ODE', "DAE", "DDE") [R package deSolve version 1.40]. In: Comprehensive R Archive Network (CRAN) [Internet]. 27 Nov 2023 [cited 22 Nov 2025]. Available: https://cran.r-project.org/web/packages/deSolve/index.html

46. Yang W, Lipsitch M, Shaman J. Inference of seasonal and pandemic influenza transmission dynamics. Proc Natl Acad Sci U S A. 2015;112: 2723–2728.

47. RCGP. Public health data. [cited 22 Nov 2025]. Available: https://www.rcgp.org.uk/representing-you/research-at-rcgp/research-surveillance-centre/public-health-data

48. Virology Dashboard. [cited 22 Nov 2025]. Available:

https://orchid.phc.ox.ac.uk/surveillance/dashboards-and-observatories-portal/virology-dashboard

49. Population estimates for England and Wales - Office for National Statistics. Office for National Statistics; 29 July 2025 [cited 22 Nov 2025]. Available: https://www.ons.gov.uk/peoplepopulationandcommunity/populationandmigration/populationestimates/bulletins/populationestimatesforenglandandwales/mid2024

Supplementary Material

Evaluation of the epidemiological outlook of the influenza A/H3N2 clade K in England during the 2025-26 season

James A Hay[*,1], Punya Alahakoon[†,1], Alexander Greenshields-Watson[†,1], Michelle Kendall[1], Mahan Ghafari[1,2], Chris Wymant[1], Robert Hinch[1], Luca Ferretti[1], Jasmina Panovska-Griffiths[1,3,4], Christophe Fraser[1]

1. Pandemic Sciences Institute, Nuffield Department of Medicine, University of Oxford, Oxford, UK
2. Department of Biology, University of Oxford, Oxford, UK
3. The Queen's College, University of Oxford, Oxford, UK
4. UK Health Security Agency, London, UK

* Correspondence to james.hay@ndm.ox.ac.uk

† Contributed equally

Supplementary figures
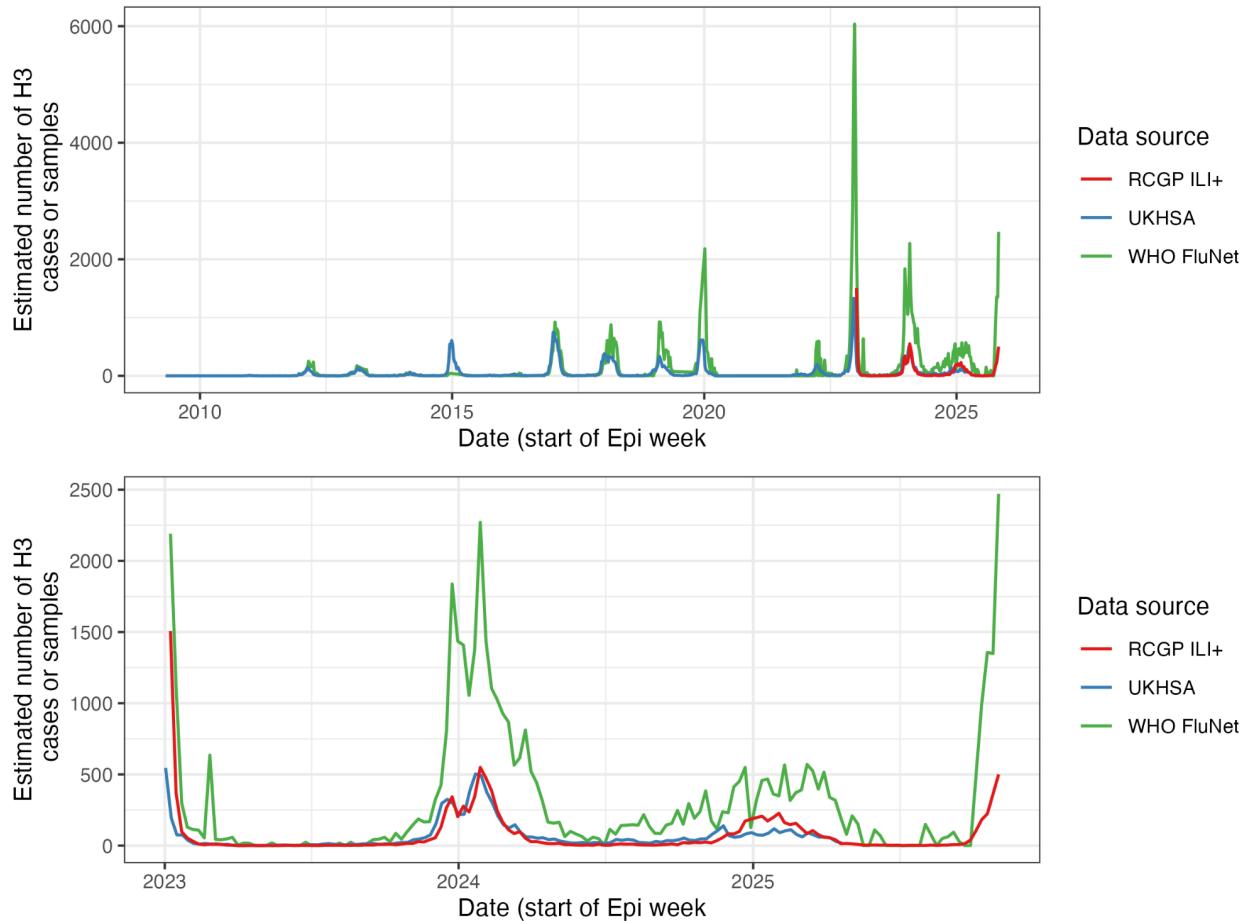
Figure S1. Comparison of the three data sources used in the analyses. RCGP = Royal College of General Practitioners Research & Surveillance Centre. UKHSA = Respiratory DataMart system. The top panel shows all data. Bottom panel zooms in on the period since 2023-01-01.
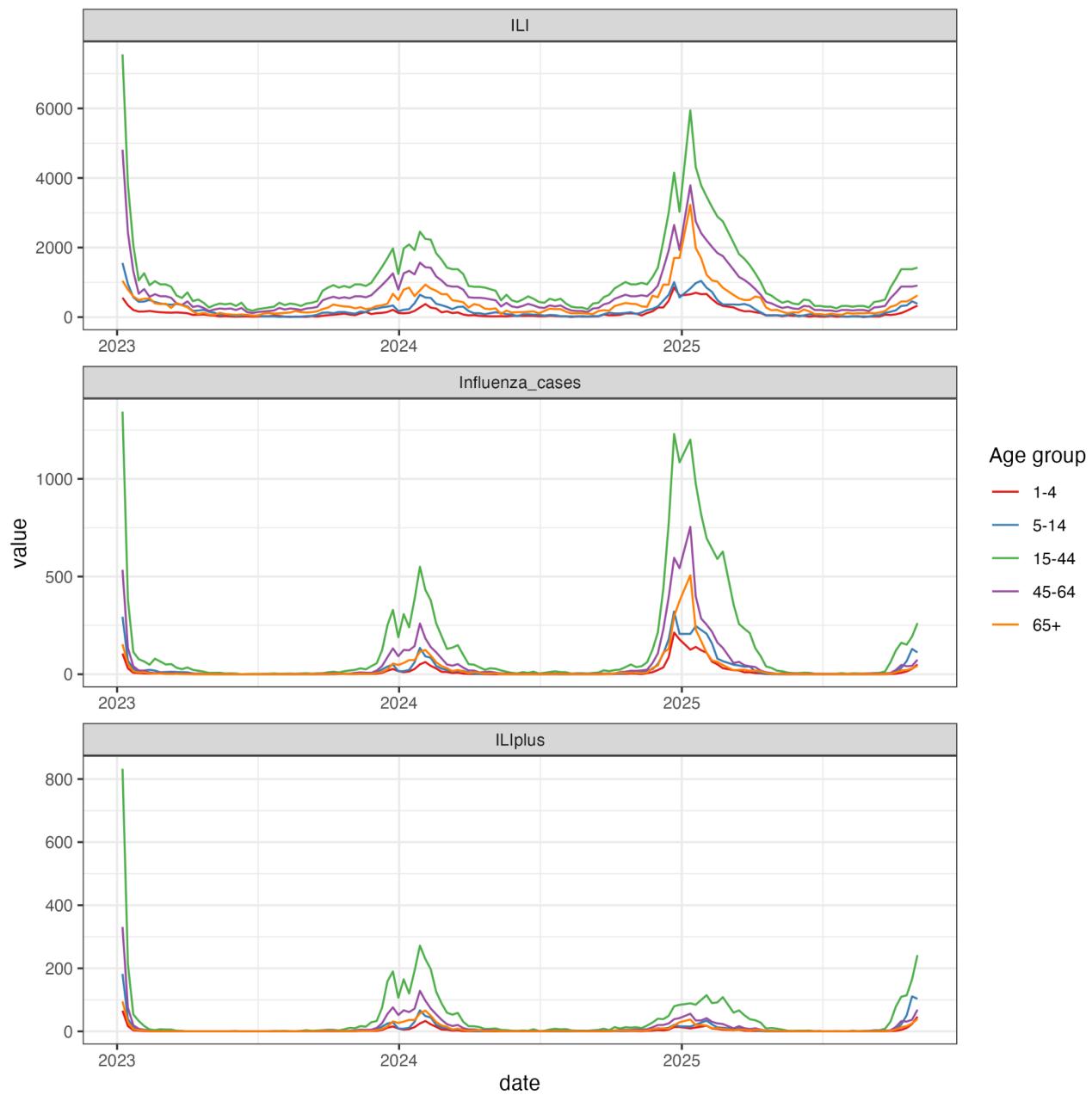
Figure S2. Comparison of age-stratified influenza surveillance indicators. Indicators: influenza-like-illness, influenza confirmed cases, and influenza A/H3N2 confirmed cases (ILI+). Data was obtained from the RCGP RSC.
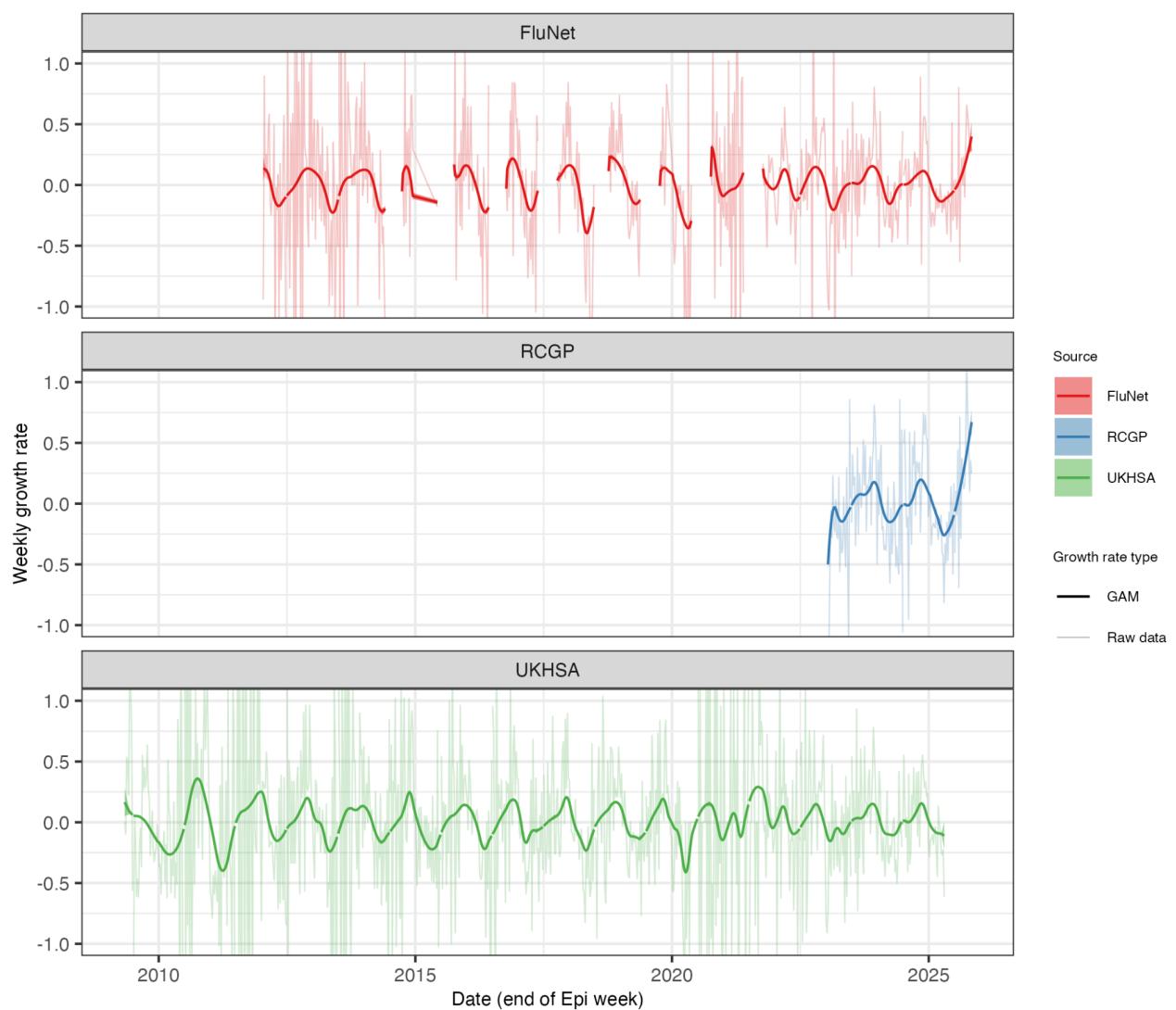
Figure S3. Comparison of weekly growth rate estimates using the three datasets. Note that the UKHSA dataset refers to Respiratory DataMart samples and does not include the 2025/26 influenza season.
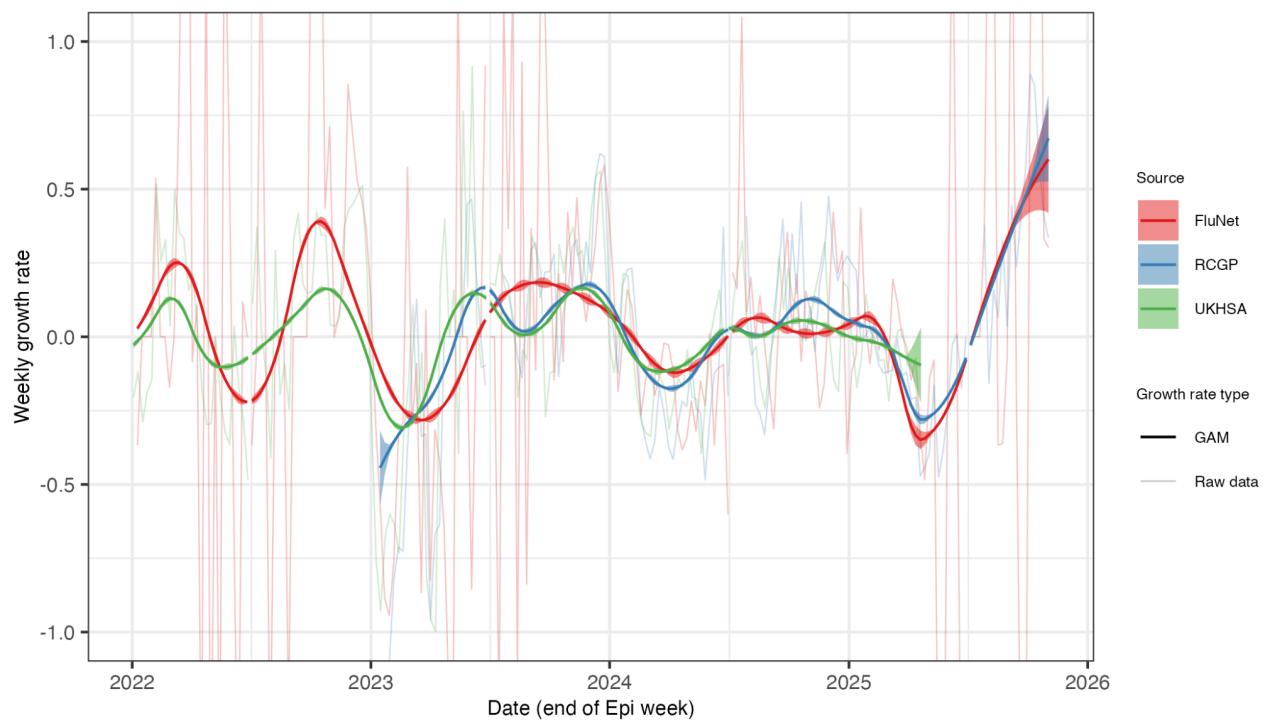
Figure S4. Comparison of recent weekly growth rate estimates from the three datasets. Note that the UKHSA dataset refers to Respiratory DataMart samples and does not include the 2025/26 influenza season.
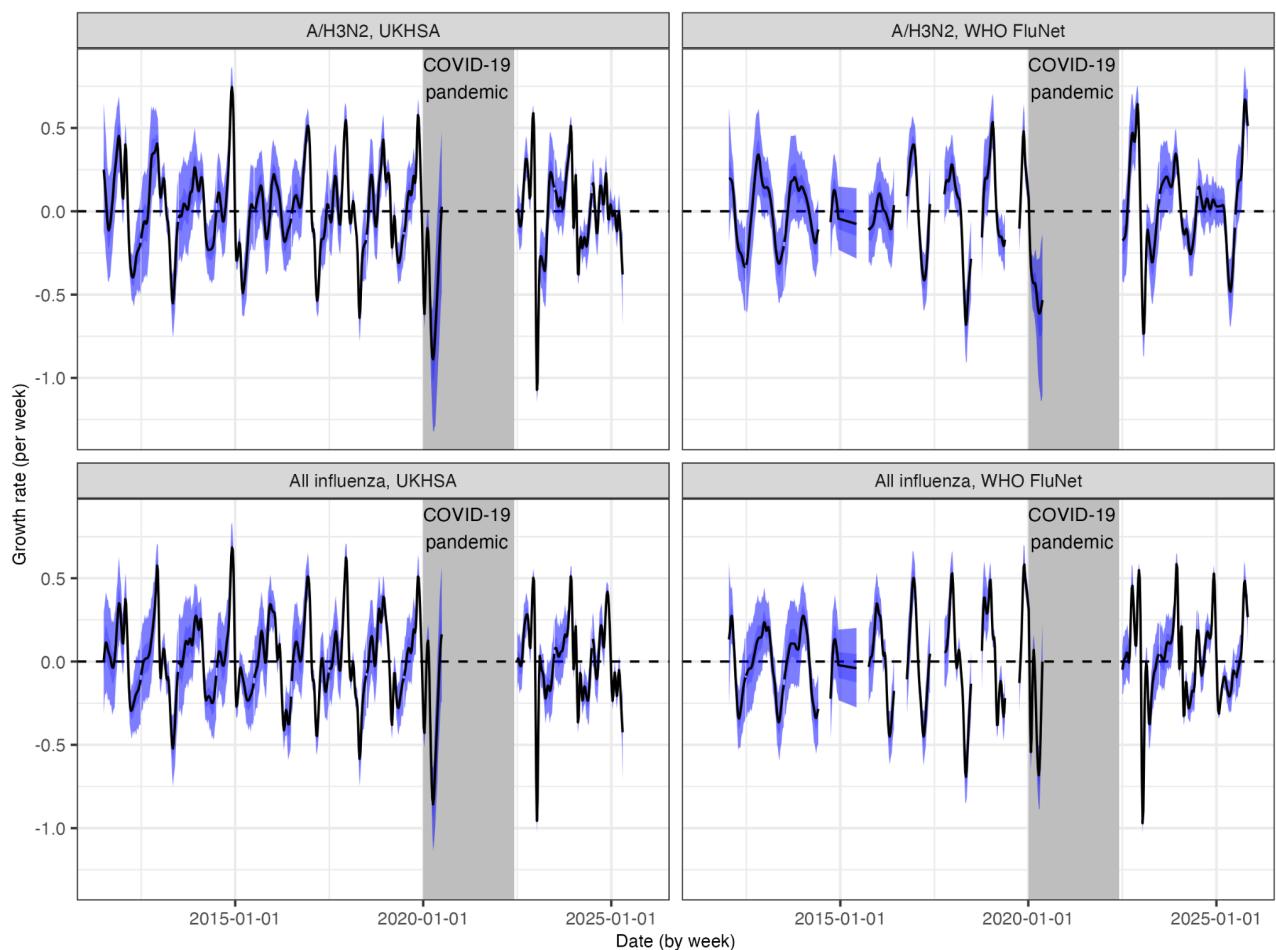
Figure S5. Comparison of weekly growth rate estimates using the EpiStrainDynamics R package fitted to UKHSA (Respiratory DataMart) and WHO FluNet samples. Shaded ribbons show posterior means, 50% and 95% credible intervals. Estimates during the COVID-19 pandemic are not shown. The top panel shows weekly growth rates of A/H3N2 samples. The bottom panel shows the weekly growth rate of all influenza samples.
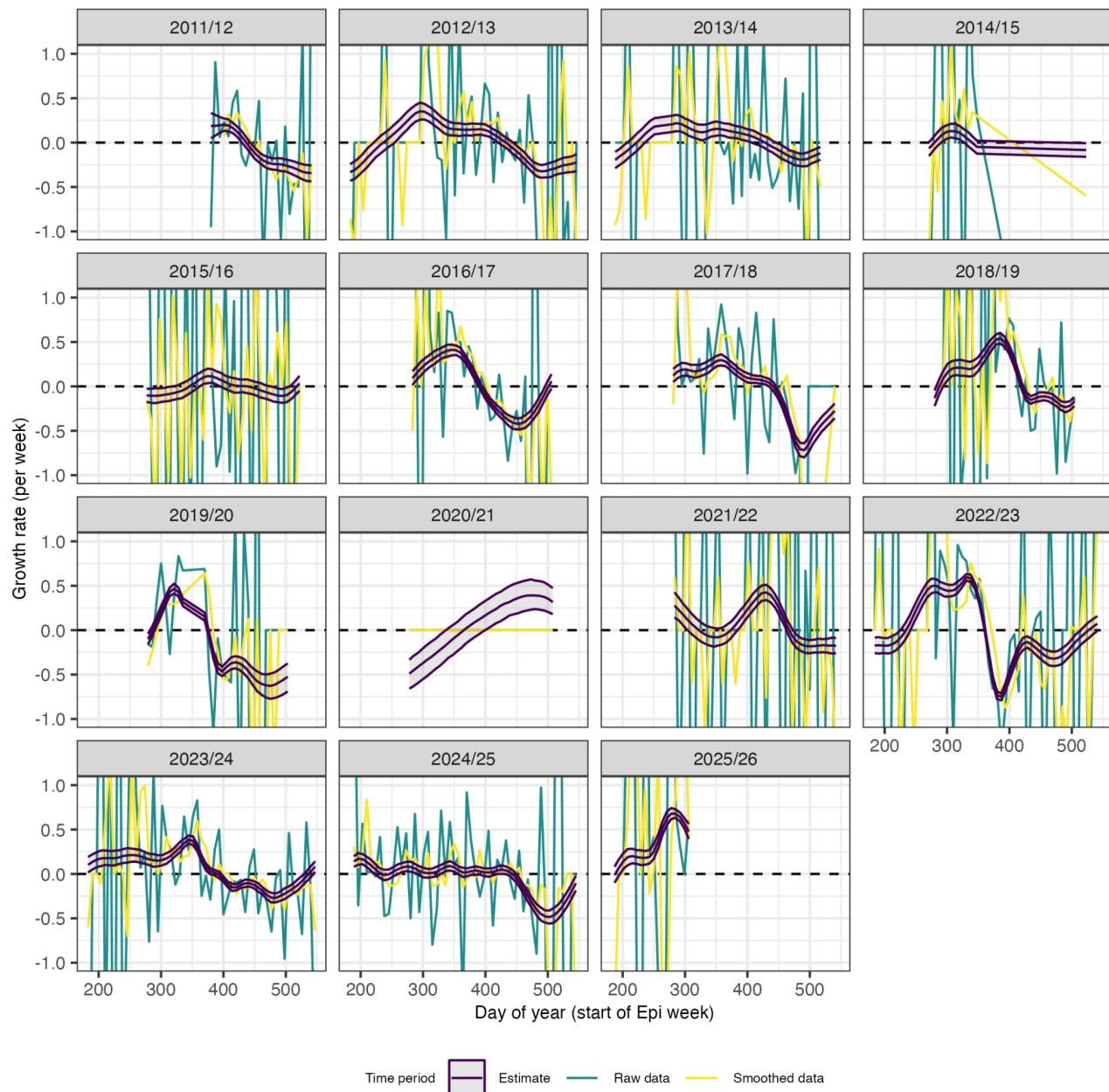
Figure S6. Fits of the penalised spline model to empirical weekly growth rates from the WHO FluNet data. Purple lines and ribbons show posterior mean and 95% CrI. The blue line shows the raw log weekly growth rates. The yellow line shows the raw log weekly growth rates smoothed over 4-week intervals (right aligned).
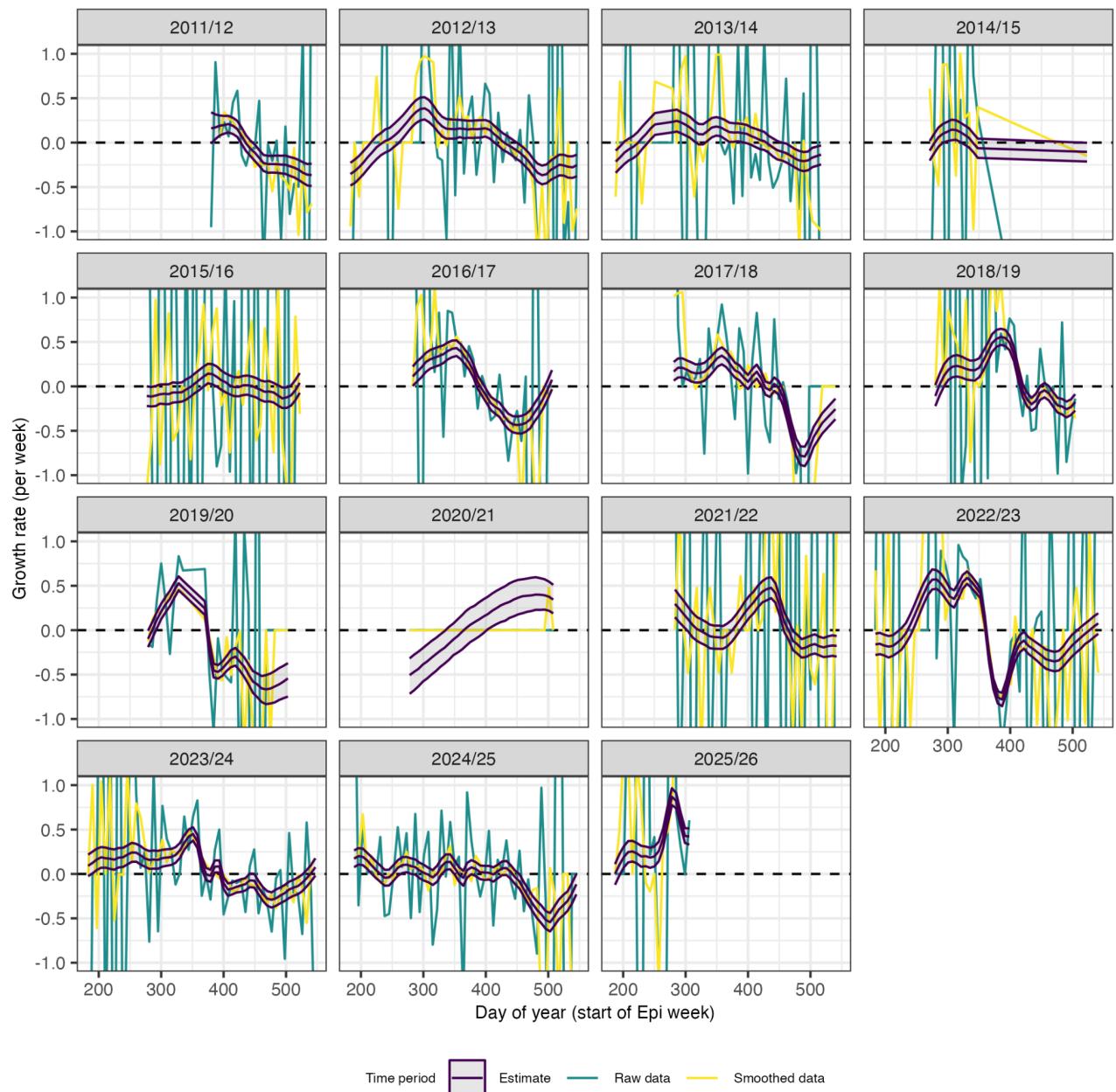
Figure S7. Fits of the random walk model to empirical weekly growth rates from the WHO FluNet data using only A/H3N2 cases. Purple lines and ribbons show posterior mean and 95% CrI. The blue line shows the raw log weekly growth rates. The yellow line shows the raw log weekly growth rates smoothed over 4-week intervals (right aligned).
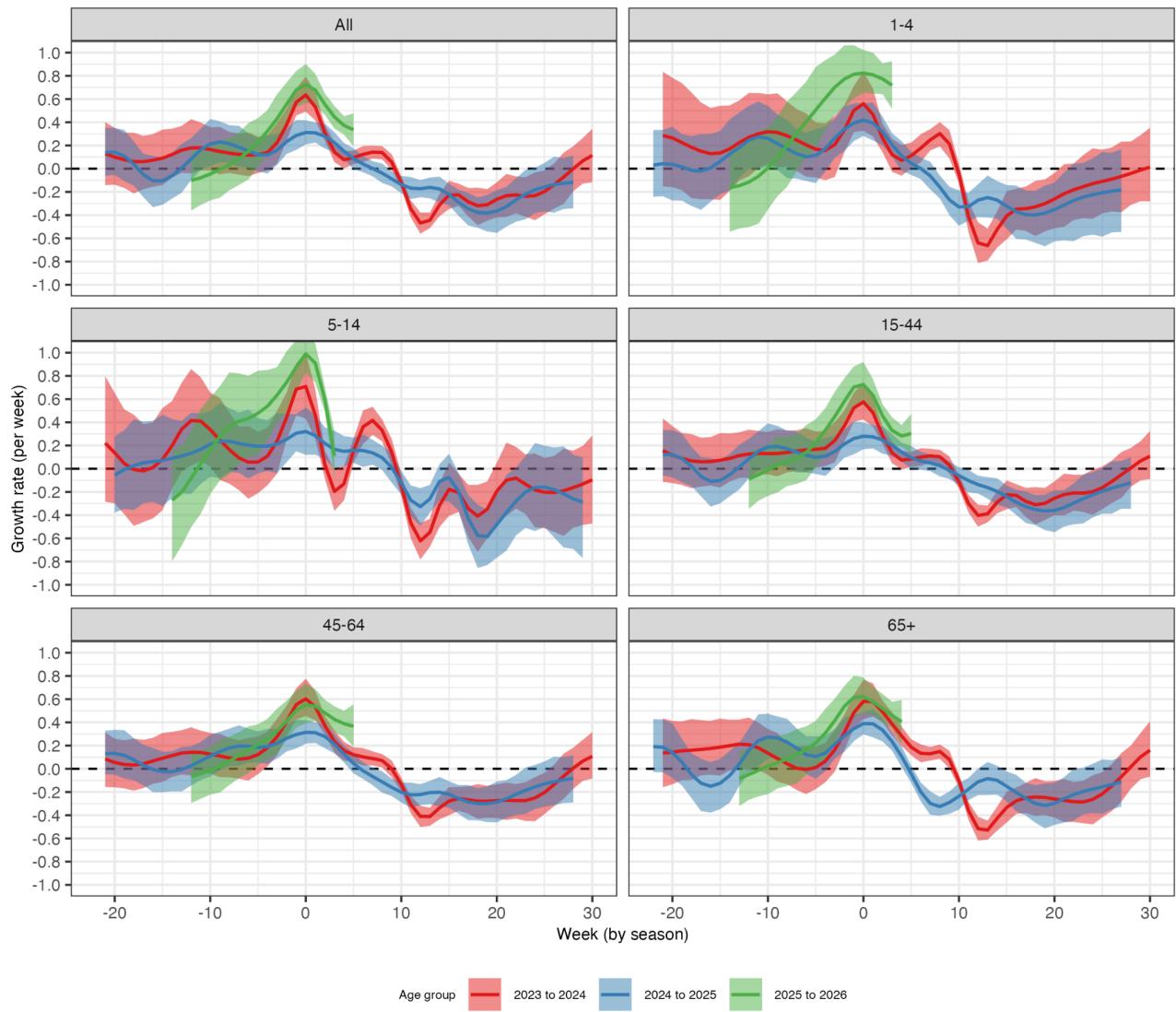
Figure S8. Growth rate estimates using a penalised spline model matching Figure 2, but instead aligned by the week of peak growth rate as x=0.
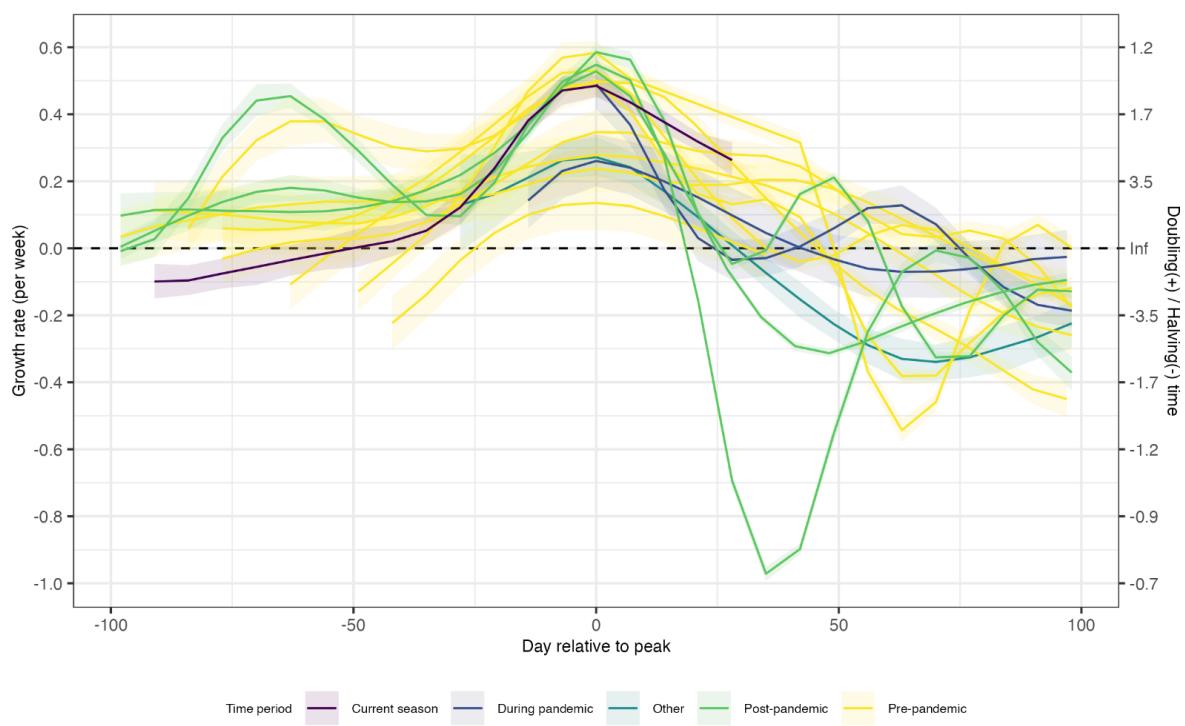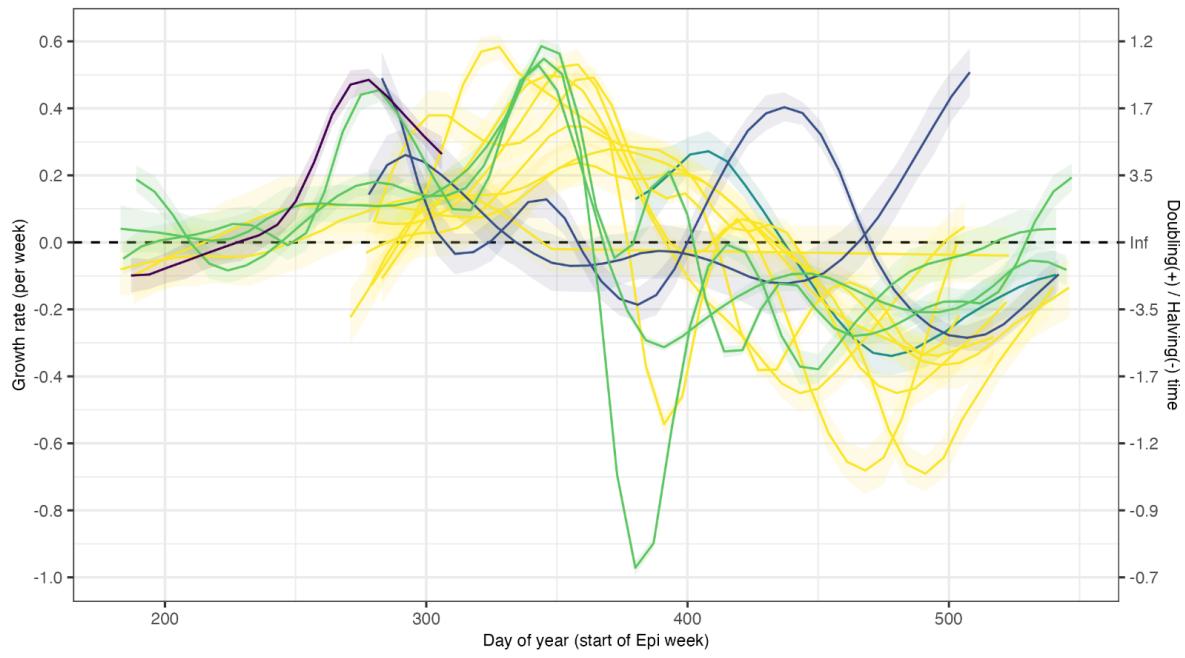
Figure S9. Growth rate of all influenza cases from the WHO FluNet database. Coloured lines and shaded regions show posterior mean and 95% credible intervals for the model-estimated weekly growth rate. Colouring distinguishes the current season from post, pre and during pandemic seasons. Doubling time is shown on the right hand y-axis.
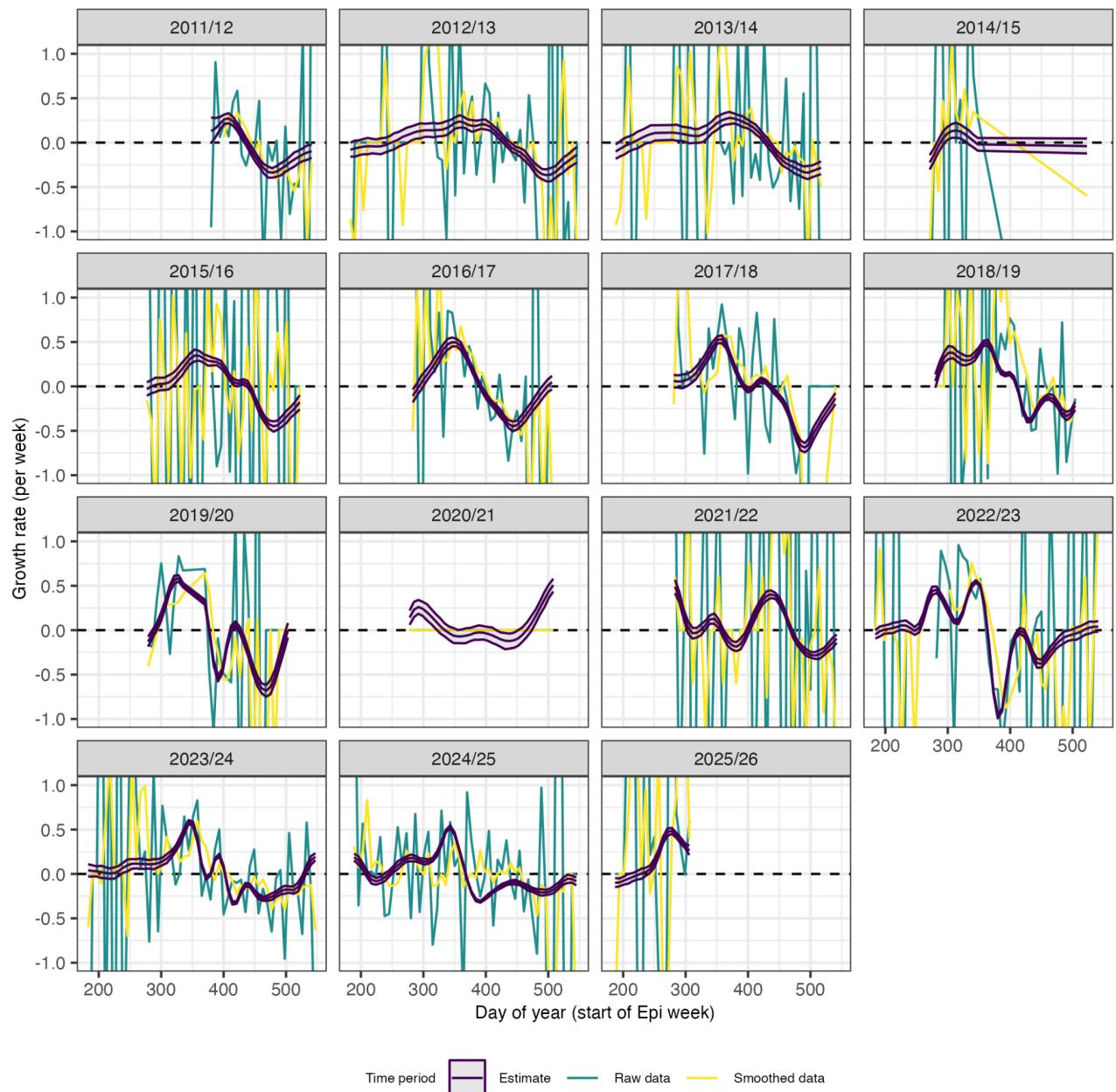
Figure S10. Fits of the random walk model to empirical weekly growth rates from the WHO FluNet data using all influenza cases. Purple lines and ribbons show posterior mean and 95% CrI. The blue line shows the raw log weekly growth rates. The yellow line shows the raw log weekly growth rates smoothed over 4-week intervals (right aligned).
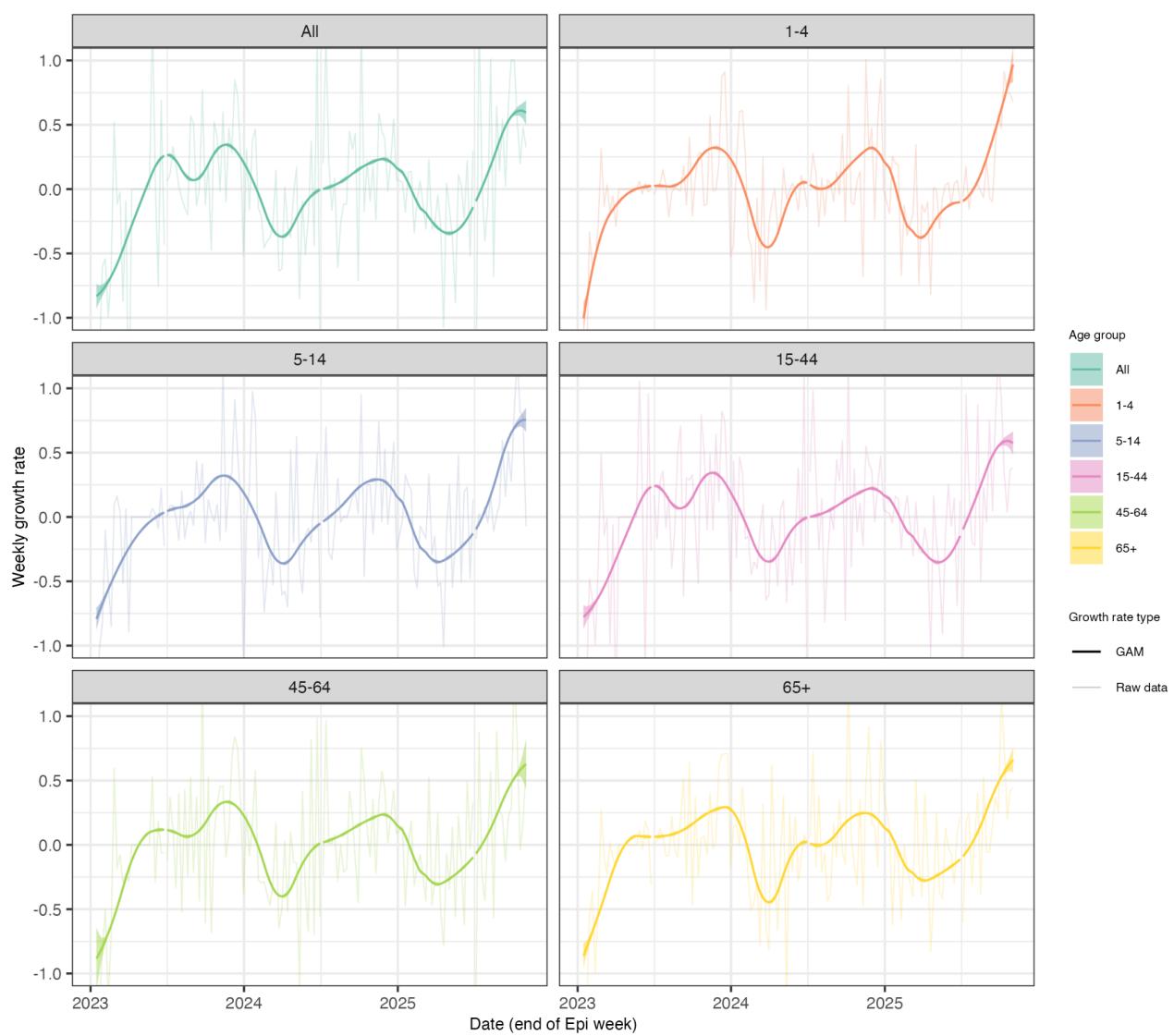
Figure S11. Growth rate estimates of age-stratified A/H3N2 cases from the ILI+ indicator matching Figure 2. Shown are the empirical growth rates and model fits using the GAM. School holidays are marked with grey bars. The autumn half-term break (i.e., the recent school holiday) is marked in red. Solid lines and ribbons show mean estimates and 95% confidence intervals.
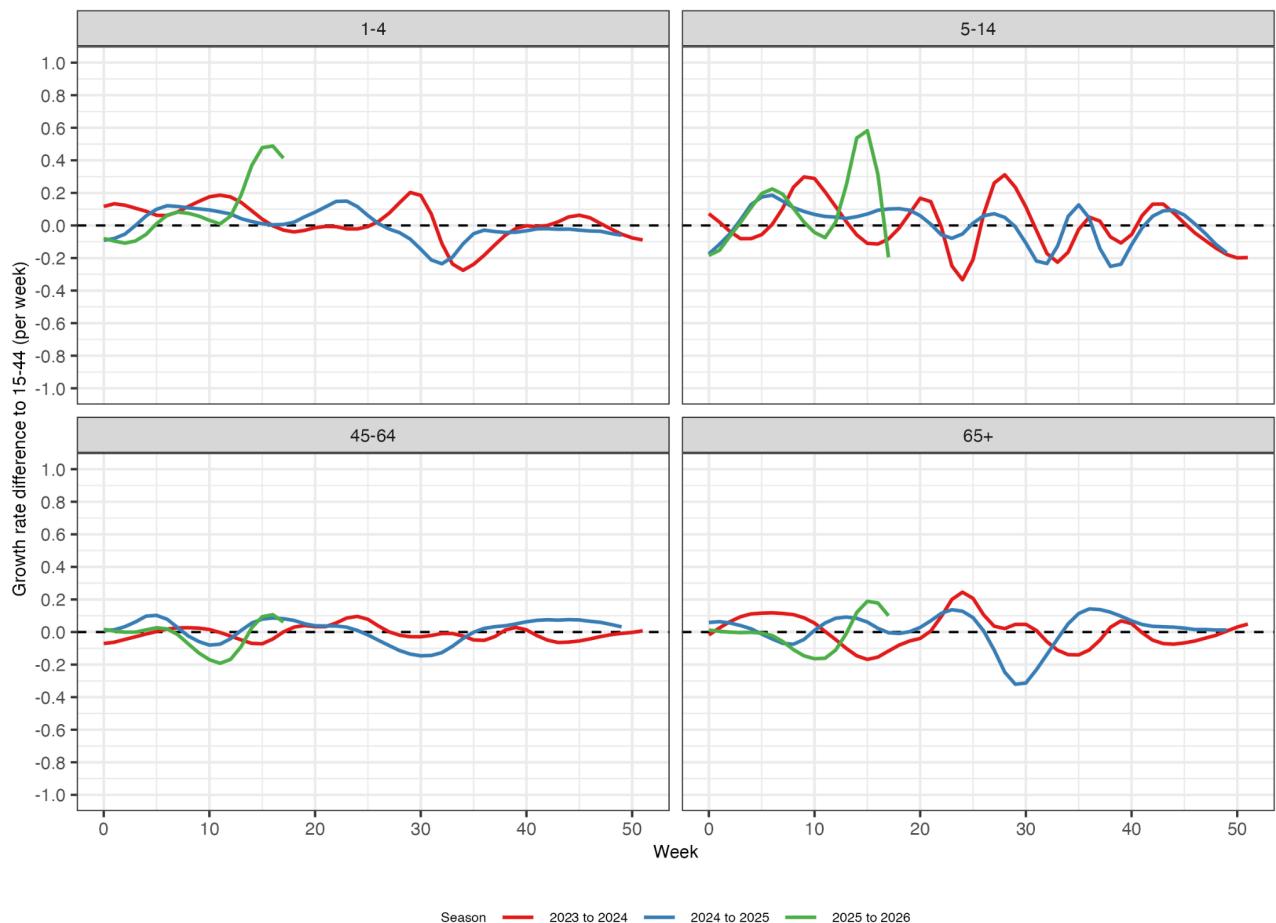
Figure S12. Comparison of age-stratified growth rates from the ILI+ indicator by season. Lines show the posterior mean estimates from the penalised spline model in Figure 2. Estimates from each season are aligned to the week since the start of the influenza season. The growth rate difference is calculated as the absolute difference between the growth rate in the focal age group to the 15-44 year old age group, such that a line significantly above 0 indicates much higher growth rates than younger adults.
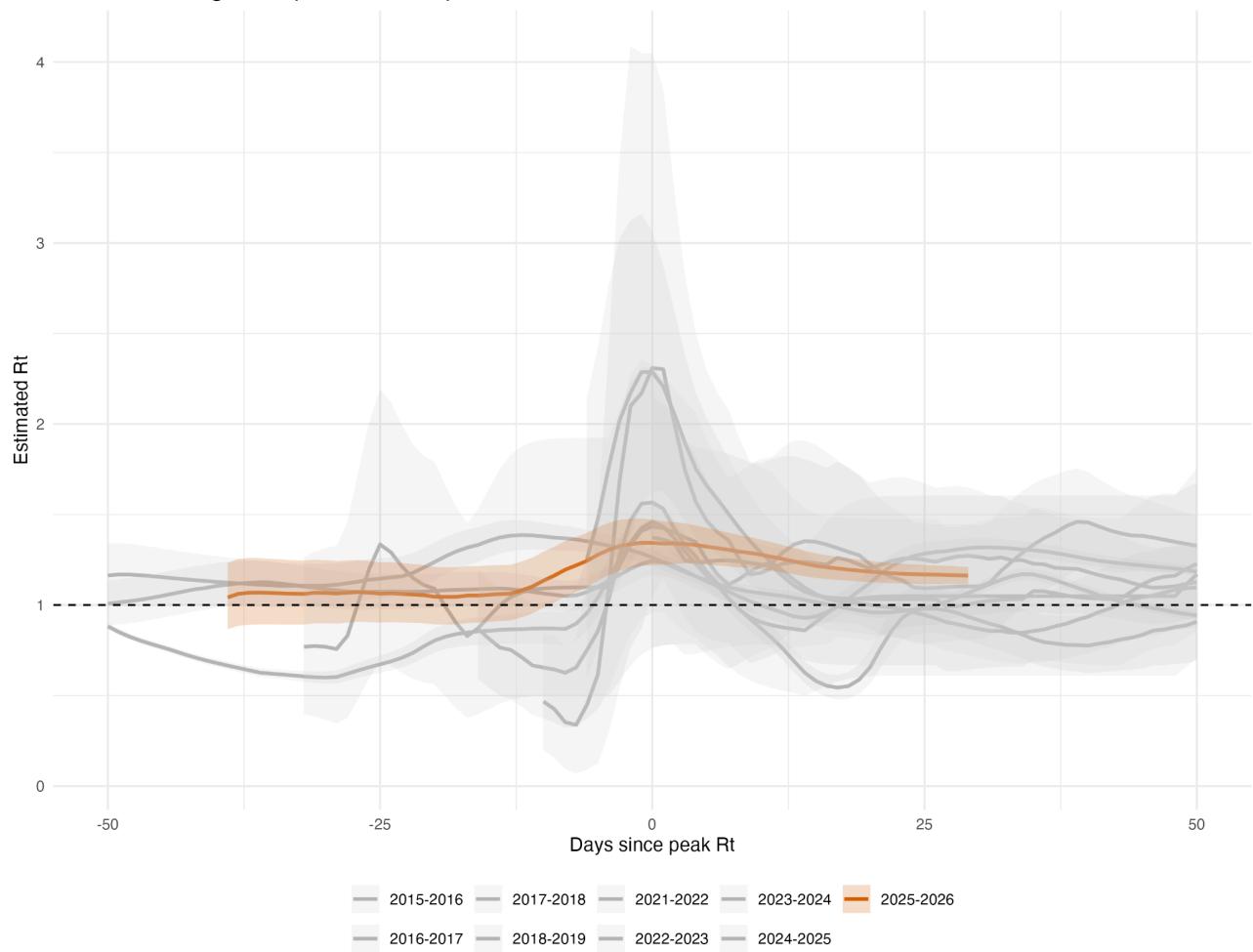
Figure S13. Effective reproduction number *(R_t)* for each influenza season arranged relative to peak pre-Christmas *R_t*. Estimates shown are identical to Figure 4, but plotted together to enable visual comparison.
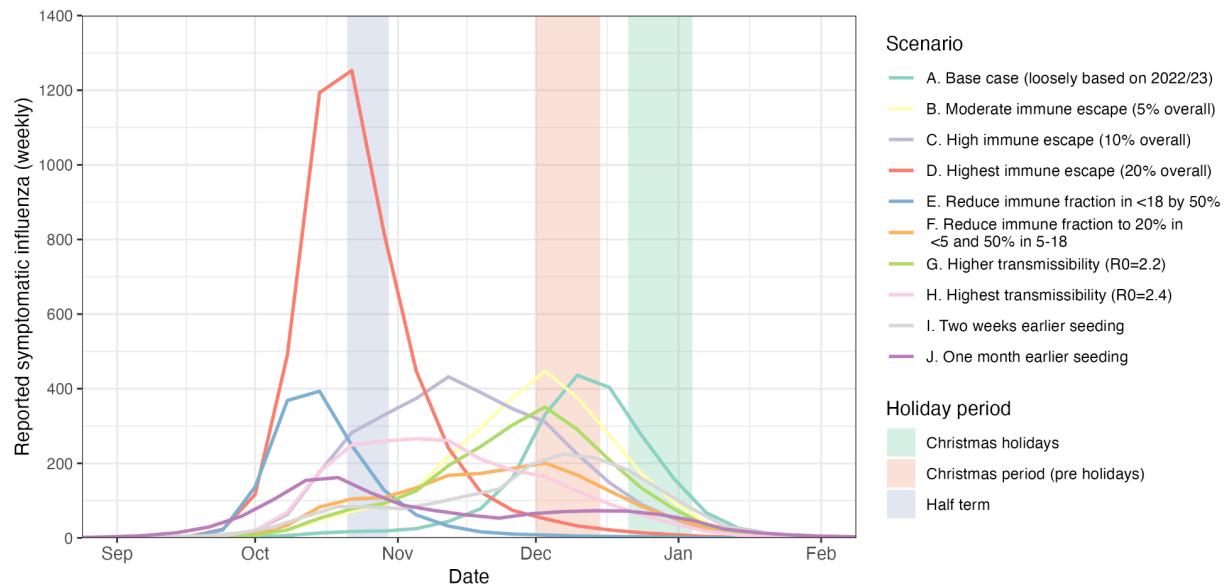
Figure S14. Comparison of symptomatic influenza incidence in 65+ from the scenario analyses shown in Figure 5.
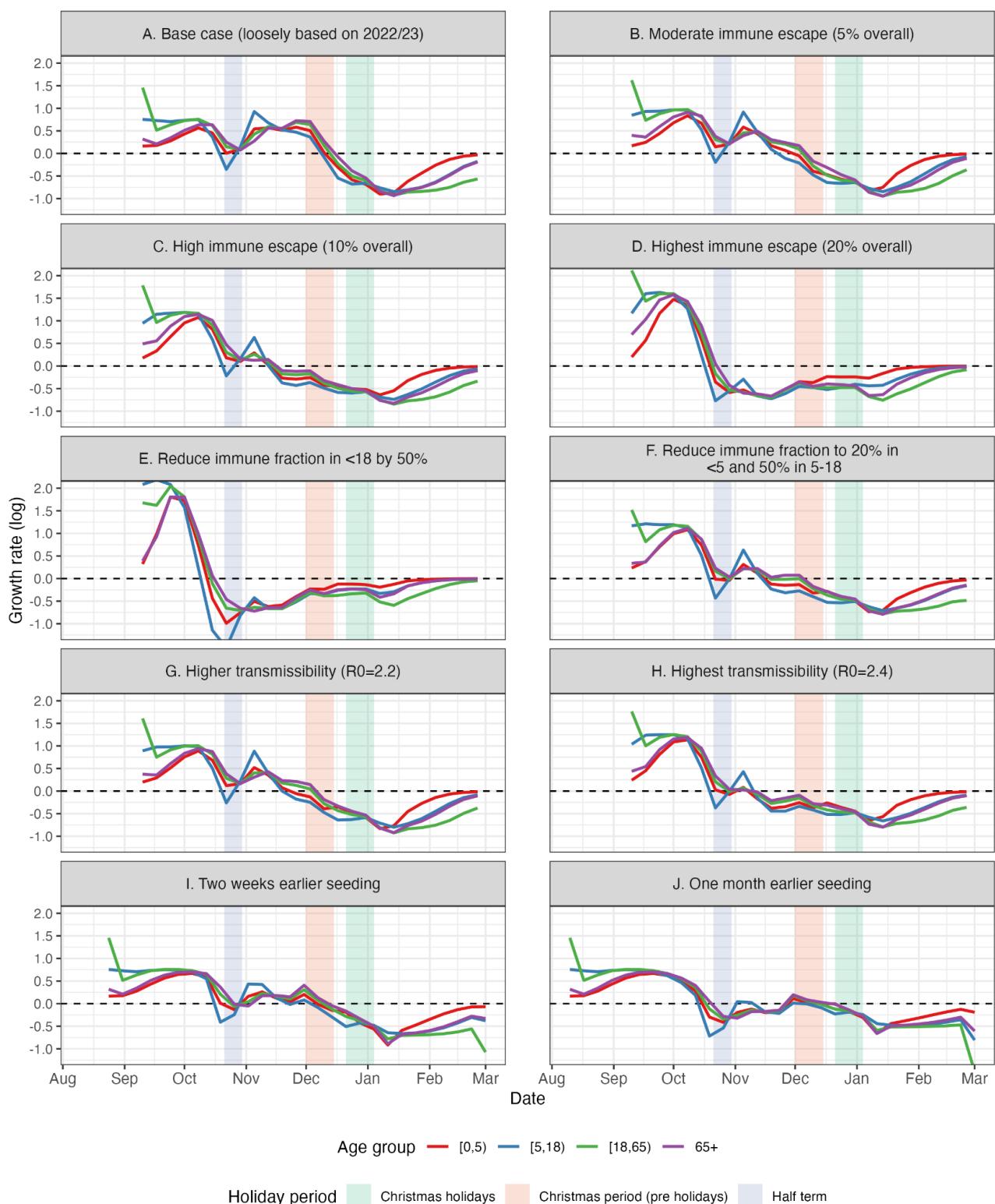
Figure S15. Comparison of weekly age-stratified growth rates from scenarios matching Figure 5.

Supplementary Methods – additional information on data sources

1. Second-Generation Surveillance System (SGSS)

Weekly influenza positivity from PCR tests by age was obtained from the UKHSA dashboard for the SGSS, available at Influenza | UKHSA data dashboard. Values are shown as a percentage of people with at least one positive PCR result for influenza (in a 7 day period). Further details are available at Data quality report: national flu and COVID-19 surveillance report - GOV.UK [36]. This dataset provided us with the proportion of tests which are positive for influenza, but not the absolute number of tests performed, proportion positive stratified by influenza subtype, nor stratification by age.

2. Royal College of General Practitioners (RCGP) Research & Surveillance Centre (RSC)

The RCGP RSC is a nationally representative primary care-based surveillance system. Weekly communicable and respiratory diseases reports are publicly available at RSC: Public health data [47]. In theory, this dataset has all of the information needed to construct an ILI+ indicator, but it is only publicly available in PDF reports and a live dashboard. The PDF reports did not contain the granularity required for the full age-stratified ILI+ indicator, and we were unable to automate digitisation of the dashboard.

We compiled weekly national incidence of influenza-like illness (ILI) rates (per 100,000 population) for England. PDF reports were downloaded for six-month intervals from January 2021 to November 2025, and Table E from each report was converted to CSV using ChatGPT-assisted extraction. These tables included age-stratified ILI rates across four age categories differing by reporting period:

1. 1-4 yrs, 5-14yrs, 15-64yrs and 65+yrs, and all ages from week 26, 2023 to week 44, 2025

2. <15 yrs, 15-64yrs, 65+yrs, and all ages for weeks 40-53, 2020, week 1, 2021 to week 5, 2021, and weeks 1-26, 2023.

This dataset provides ILI rates by age, which we convert to estimates for absolute ILI case numbers by multiplying by the population size per age group. However, it does not stratify ILI into influenza A/H3N2 positivity.

We also digitised data on the total number of samples tested and the number of samples positive for influenza by age group for the 2022 to 2023 influenza season and used this to calibrate the base case for the scenario analyses. We did not digitise the subtype-specific testing fraction by age group, and thus this particular dataset used all influenza cases by age [48].

3. Respiratory DataMart sentinel system for hospital testing.

The Respiratory DataMart is a sentinel laboratory surveillance system which monitors all major respiratory viruses in England, compiling data from 17 contributing laboratories. Participating laboratories test swabs for respiratory viruses, including influenza A viruses, using real-time polymerase chain reaction (RT-PCR), though not all laboratories test for or report all viruses. The absolute number of samples in this system is much lower than SGSS, but gives absolute numbers of tests rather than just percentage positive.

We used data from the Respiratory DataMart in two ways:

1. We obtained weekly influenza surveillance data from the UK Health Security Agency (UKHSA) annual influenza reports for the 2024 to 2025 influenza season and the 2023 to 2024 season (available at [Influenza in the UK, annual epidemiological reports - GOV.UK](#)). This dataset contained the weekly number of influenza detections by subtype and the overall percentage positive for influenza stratified by age group.
2. The winter 2024 to 2025 report contained data from 2017 to 2025, while the winter 2023 to 2024 report contained data from 2009 to 2024. We created a combined dataset spanning the period 27 April 2009 to 1 April 2025. This dataset included weekly counts of laboratory-confirmed influenza cases by subtype: influenza A (not subtyped), influenza A(H1N1)pdm09, influenza A(H3N2), and influenza B. Additionally, the dataset provides the overall percentage of specimens testing positive for influenza. However, these datasets were not stratified by age group.

4. World Health Organisation (WHO) FluNet

Weekly counts of reported influenza specimens were obtained from the WHO FluNet platform [19]. This is the global influenza virological surveillance system collecting weekly sentinel and non-sentinel (e.g., outbreak investigations, point-of-care testing) surveillance data from national influenza centres. Data was extracted for the period September 30, 2013, to November 6, 2025, restricted to England and non-sentinel surveillance sites. Although the non-sentinel sites are less systematic than sentinel networks, they provide substantially larger sample sizes, which are advantageous for estimating growth rates. The extracted dataset included the weekly number of samples classified as A(H3), influenza A (not subtyped), A(H1N1pdm09) influenza B, and overall influenza cases. We allocated the unsubtyped influenza A cases into A/H3N2 and A/H1N1 cases proportional to the ratio of subtyped samples.

Aligning mismatched age groups from different datasets

Where age groups were misaligned, we re-distributed metrics (such as ILI or percentage positive for influenza) into new age bandings by assuming that each metric is the same for all ages (in years) within an age group. We then recombined datasets into new age bands by reweighting these age metrics based on the age distribution of England [49].

Additional analyses of Respiratory DataMart data
In Figures A1 and A2, we compare age-stratified trends in the number of influenza positive samples between the current 2025/26 season (up to 6th November 2025 – analyses outdated) and the 2022/23 season, which was also A/H3N2 dominated and showed similar dynamics. Note that in the 2022/23, the oldest age group was reported as 65+ years, whereas in the 2025/26 season the 65-79 and 80+ year old age groups were reported separately. For each, we report here only the age groups <65 years. The age-stratified positivity trends appear very similar between the 2022/23 and 2025/26 season, though the earlier increase in younger ages is still apparent. Age-stratified growth rates are similar though it's hard to be precise with these data.
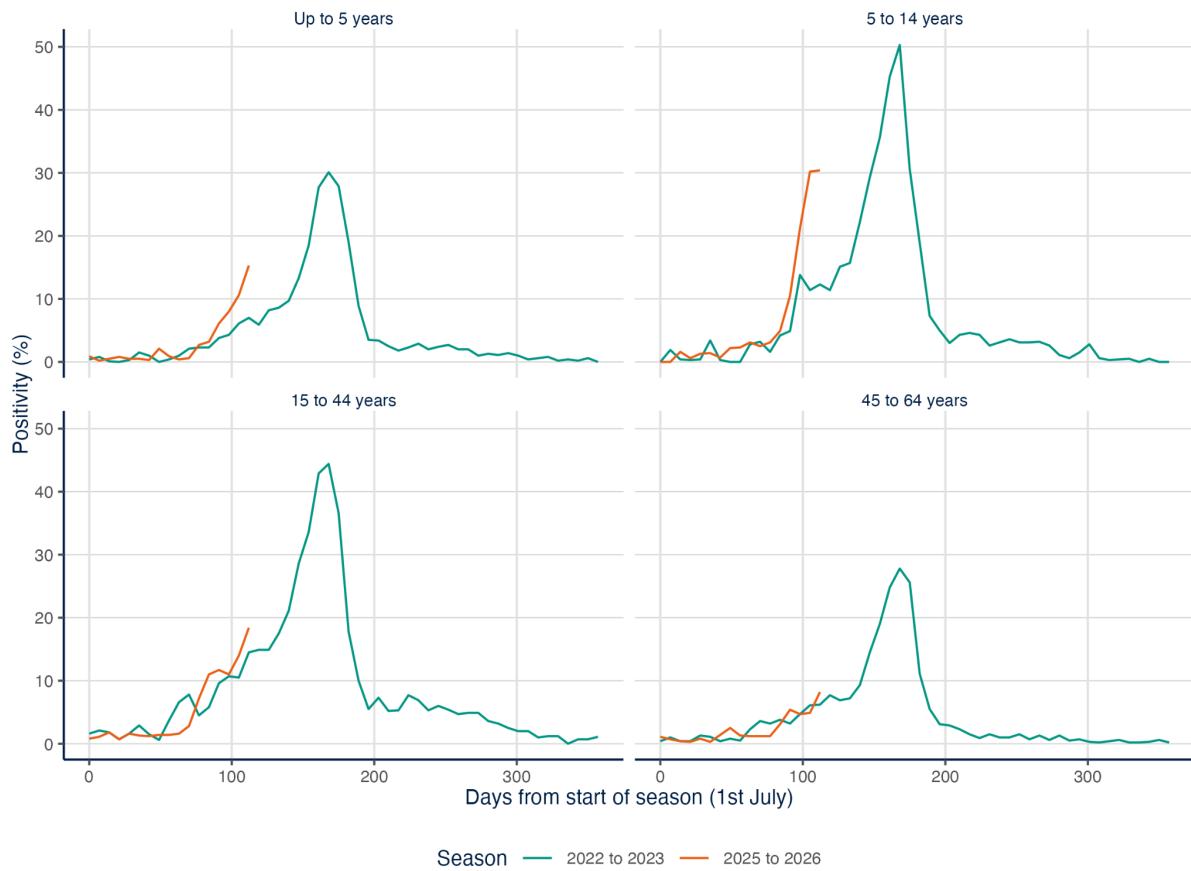
Figure A1. Influenza positivity % from the Respiratory DataMart system by age group for the 2022/23 and 2025/26 seasons.
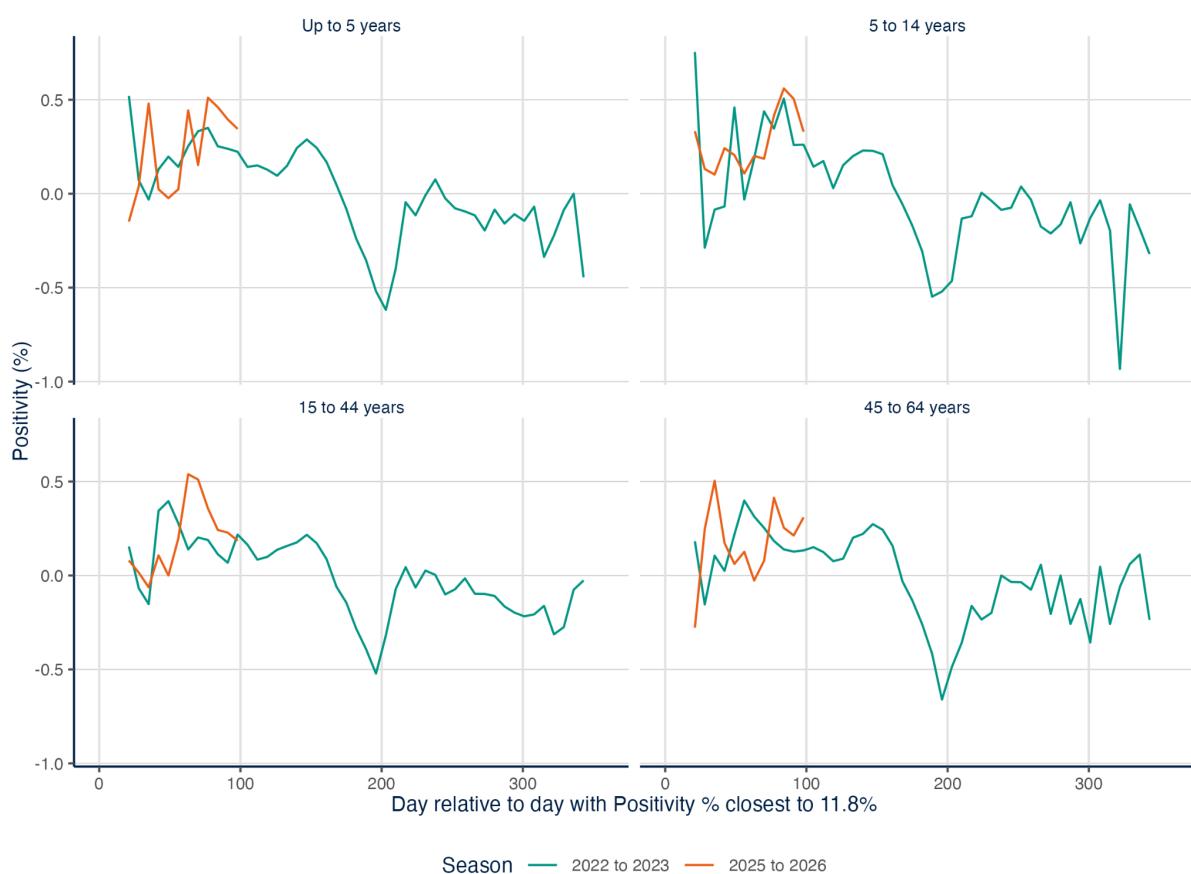
Figure A2. Growth rate of influenza positivity % from the Respiratory DataMart system by age group for the 2022/23 and 2025/26 seasons.